Effect of H_2 Fuel-Addition and Air-Side CO_2 Dilution on the Stabilization of Turbulent Dutch Natural Gas Jet Diffusion Flames

Eduard van Haren

TU Delft

Effect of H_2 Fuel-Addition and Air-Side CO_2 Dilution on the Stabilization of Turbulent Dutch Natural Gas Jet Diffusion Flames

by

Eduard van Haren

to obtain the degree of Master of Science
at the Delft University of Technology,
to be defended publicly on Friday July 5, 2019 at 14:00.

P&E Report number:	2985	
Student number:	4291743	
Project duration:	September, 2018 – July 2019, 2019	
Thesis committee:	Dr. Ir. Mark Tummers,	TU Delft, Supervisor
	Prof. Dr. Ir. Sikke Klein,	TU Delft
	Prof. Dr. Dirk Roekaerts,	TU Delft

An electronic version of this thesis is available at `http://repository.tudelft.nl/`.

TU Delft

Preface

This thesis concludes my MSc Mechanical Engineering study at the TU Delft. The research is conducted at the Fluid Mechanics section of the faculty of 3ME. I would like to thank the people that contributed to this work and the thesis process.

Foremost, I would like to thank Mark Tummers for his guidance, patience and that I could always drop by for a chat. Great gratitude goes out to Bart Hoek, helping me out with the experimental work and for the interesting discussions on various topics. Johan Steimes provided me a great kick-start in the thesis-project, thanks a lot for the guidance in the first half of the project. Furthermore I want to thank the people of the Fluid Mechanics section; the PhD students, the staff and Caroline Legierse. I enjoyed the coffee breaks at 10:00 and the Panta Rhei Candy Shop helped me to find that little extra motivation. Apart from the thesis work, I owe many of the valuable experiences in my study period to Marion Faludi from the 3ME International office, thanks!

Eduard van Haren
Delft, June 2019

Abstract

The turbulent lifted Dutch natural gas jet diffusion flame in cold co-flowing air is widely used in gas turbine operation and subject of the current investigation. In striving to clean and sustainable combustion, adding hydrogen to the Dutch natural gas (DNG) fuel and CO_2 in the coflow is promising.

Objective of this investigation is to study the effect of hydrogen fuel-addition and CO_2 coflow-dilution on the stability of a turbulent lifted DNG jet diffusion flame in cold co-flowing air. OH* chemiluminescence and particle image velocimetry (PIV) are applied simultaneously at a low sampling frequency of 50 Hz to determine time-averaged statistics of the lift-off height and stabilization point location of the flame. PIV measurements at a sampling frequency of 2.5 kHz are performed to determine the transient behaviour of the stabilization point, the flow conditions at the stabilization point and the burning velocity.

Hydrogen fuel-addition leads to increased flame stability. With more hydrogen in the fuel, the lift-off height reduces and the stabilization point location shifts upstream and radially inward. The burning velocity at the stabilization point increases with increasing hydrogen fuel-concentration. A significant difference is observed in the burning velocity conditioned on upstream or downstream stabilization point motion. Hydrogen enables the flame to stabilize in a region of the flow that is characterized by high gas velocity and high vorticity.

CO_2 dilution of the coflow leads to decreased flame stability. With increasing CO_2 coflow-dilution, the lift-off height increases and the stabilization point position shifts downstream and radially outward. The burning velocity at the stabilization point increases with increasing CO_2 coflow-dilution and the flame stabilizes in a flow region with significant lower vorticity.

Additionally, this report provides useful statistics of the investigated quantities and presents a description for the transient behaviour of the stabilization point.

Contents

1 Introduction

1.1. Background of the Investigation

Nowadays society faces the challenge of an increasing clean energy demand. Growing population and increasing wealth lead globally to more energy usage [1]. Carbon based fossil energy sources are currently the key energy provider [2]. However fossil fuels are becoming more scarce [3] and new energy solutions have to be sought. Current energy supply largely comprises of combustion-based conversion, responsible for the emission of vast amounts of hazardous pollutants and greenhouse gasses. Combustion emissions can be categorized in globally and locally affecting emissions. In the first category is the greenhouse gas CO_2. It is thought that CO_2 emission lead to global warming. Current energy supply is therefore the main contributor in the global warming problem [4]. The other category of emission products cause local problems. These are combustion products as NO_x, SO_x, CO, fine particles and unburned hydrocarbons. Local emission products can cause health issues and pollute the local environment. For this reason, emission reduction receives increasing attention, which calls for new combustion technologies to reduce pollutant emissions. Therefore it is necessary to explore new energy technologies to secure a stable and clean future energy supply.

Combustion is widely used to convert fuel in useful forms of energy. It is one of the oldest technologies and still is of paramount importance as 90% of worlds energy is converted by combustion [5]. Improving combustion practice and exploring new combustion technologies is therefore part of the search for sustainable clean energy supply. The focus of modern research in combustion technology research is to reduce pollutant emissions. Improvements can be realized by using clean renewable fuels and utilizing advanced combustion techniques.

From the fuel point of view, renewable carbon- and sulphur-free fuels can be used in combustion. Renewable fuels are formed from infinite available energy sourcing from sunlight or wind. These fuels act as energy storage medium of sustainable energy. Hydrogen, H_2, is such a fuel and is expected to be a potential future sustainable fuel [6]. Currently, the share of wind and solar energy is increasing and receives a lot of societal, economical and technological attention. In the Netherlands, several wind and solar parks are recently developed or are currently under development. There is high potential to store wind and solar energy in hydrogen through the electrolysis of water. Hydrogen would be effective in peak-shaving the energy demand and supply in periods of electrical energy over-demand. Compared to the combustion of hydrocarbon fuels, hydrogen combustion is much cleaner. Combustion of the former leads to the emission of unwanted species as CO_2, CO, NO_x, soot, SO_x and unburned hydrocarbons, whereas the latter only emits NO_x at high combustion temperatures.

Gas turbines are used to provide heat and power and are fuel-specific designed, in the Netherlands for Dutch natural gas. Therefore, gas turbines are in their current state not able to combust pure hydrogen. As operation on pure hydrogen would imply complete redesign of the combustion equipment, hydrogen addition to hydrocarbon fuels is promising and feasible on the short term by adapting existing equipment. Next to this, considerable experience is available in the use of hydrogen and hydrogen containing fuels as it is heavily used in industry as energy carrier and chemical feedstock. Hence, hydrogen addition is a logical first step on the short term striving to clean energy production [7].

Meanwhile, research towards emission reduction and increasing the energetic efficiency of combustion is critical in shifting towards clean and sustainable energy. One of the techniques to realize this is external exhaust gas recirculation, commonly abbreviated by EGR. This technique can be applied in gas turbine systems of combined heat and power plants (CHP) to enable the operation at deep part load while maintaining low emissions [5] and high efficiency. This as gas turbines are optimized to operate in a narrow range of operational conditions. Part load gas turbine operation is expected to be critical in future energy mix in The Netherlands, as gas turbines are expected to provide the energy base load next to renewable but intermittent energy sources. Gas turbines should be able to reduce their energy production quickly in case of a peak in the supply of renewable energy. Exhaust gas recirculation provides the oxidizer stream with inert gasses, mainly CO_2. Combustion exhaust gasses are extracted from the combustion chamber and intercooled. It is then recirculated and mixed with freshly in-flowing combustion air, after which it is fed in the combustion chamber of the gas turbine.

1.2. Objectives of the Research

The turbulent lifted jet diffusion flame is widely used base in gas turbine operation. Stability of such a flame is important for safe and reliable operation of a gas turbine. Yet, there is currently no consensus on the leading stabilization mechanism of the turbulent lifted jet diffusion flame and various stabilization concepts are proposed over time. This hampers the use of a renewable fuel like hydrogen or the application of EGR in gas turbines.

The objectives of the present investigation are to determine the effects on the stabilization mechanism of a turbulent lifted jet diffusion flame of (1) hydrogen addition to the DNG base fuel and (2) CO_2 dilution of the cold coflow combined with hydrogen fuel-addition. In particular, attention will be focused on the lift-off height, the stabilization point position (including its transient behaviour), the flow conditions near the stabilization point, and the burning velocity.

1.3. Outline of the Report

Chapter 2 presents the current research state in form of a literature review. This chapter also positions the current research in the existing scientific landscape. Chapter 3 describes the experimental setup that was used in this study as well as the investigated flames. Chapter 4 presents the results concerning the methodology used to extract information on the stabilization characteristics of the different flames from the experimental data. Chapter 5 presents and discusses the results. Finally, in chapter 6 conclusions are drawn and recommendations are given to on future research in this field.

2

Literature Review on Stabilization of Turbulent Lifted Jet Diffusion Flames

Lifted flames are used in a combustion chamber of a gas turbine to prevent nozzle damage of the burner. Figure 2.1 sketches a two-dimensional cross section of a lifted jet diffusion flame. The fuel is issued from the long pipe in the middle into a cold oxidizer coflow. Mixing of fuel and oxidizer occurs and the stoichiometric contour is visualized in 2.1.

An important flame quantity in flame stabilization is the flame speed. The flame speed is the velocity of the flame front relative to the unburned fuel-oxidizer mixture. The laminar flame speed S_L is this velocity if the fuel is mixed to stoichiometric conditions. The laminar flame speed can be interpreted as a characteristic of a specific fuel-oxidizer mixture.

The turbulent flame speed S_T is related to the laminar flame speed S_L by assuming that the turbulent flame is a wrinkled laminar flame. Figure 2.2 shows an illustration of the wrinkled flame front with the mean area of the turbulent wrinkled flame front A_T and the mean area of the laminar flame front A_L. Conservation of mass leads to the definition of the turbulent flame speed as

$$S_T = S_L \frac{A_L}{A_T}. \tag{2.1}$$

Damköhler proposes a relation between the mean turbulent and laminar flame front as in $A_L/A_T = 1 + \frac{S'}{S_L}$ [5]. Including this in equation 2.1 results in a final relation of the turbulent flame speed as function of on the laminar flame speed S_L and the turbulent fluctuation of the flame speed S'

$$S_T = S_L \frac{A_L}{A_T} = S_L(1 + \frac{S'}{S_L}) = S_L + S'. \tag{2.2}$$

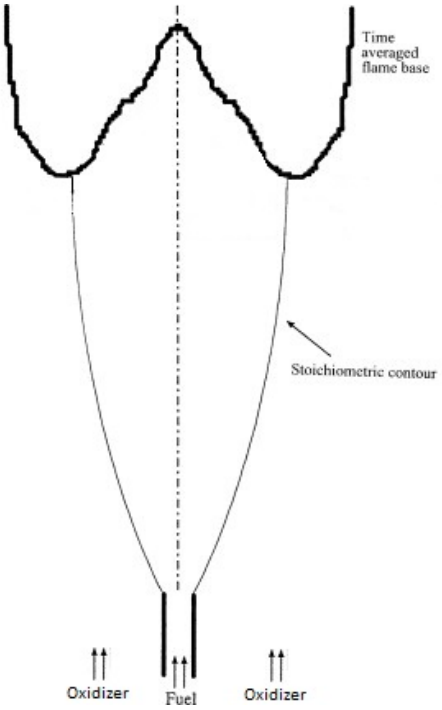

Figure 2.1: Schematic of a turbulent lifted jet diffusion flame in cold oxidizer coflow, adapted from [8].

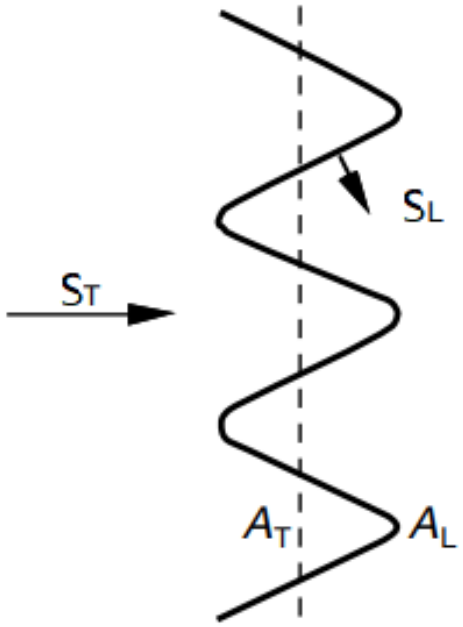

Figure 2.2: Wrinkled flame concept with the respectively turbulent and laminar flame speed v_t and $v_l l$ plus the mean areas A_t and A_l of the turbulent and laminar flame front respectively, adapted from [5].

2.1. Stabilization Concepts

The review article by Lyons [9] discusses the different flame stabilization theories that were proposed over time and divided these into five categories.

1. **The Critical Scalar Dissipation Concept**

   Peters and Williams [10] argue that a turbulent non-premixed flame is made up of strained laminar flamelets. Flamelets are considered thin laminar reaction sheets in turbulent flow. If the strain on these laminar flamelets exceeds a certain level, the flamelet is extinguished. Stabilization occurs at a position where the scalar dissipation rate does not impose enough strain to extinguish the local flamelets. This forms a stable flame front consisting of laminar flamelets. Lyons [9] disputes the link between the scalar dissipation rate and flame extinguishing as partial premixing upstream the flamefront and short-living localities of very high scalar dissipation are not taken into account.

2. **Turbulence Intensity Concept**

   This theory points that the turbulence intensity impacts flame stabilization as the turbulence influences the local flame speed. It is assumed the flame stabilizes if the local turbulent flame speed equals the local gas velocity.

3. **Premixed flame concept** In the premixed flame concept formulated by Vanquickenborne and van Tiggelen [11] it is assumed that the base of a turbulent lifted diffusion flame is sufficiently mixed to stoichiometric conditions such that it can be considered as a premixed base. In the premixed base the turbulent flame velocity equals the gas velocity, thus stabilizing the flame. This concept is visualized in figure 2.3. Lyons [9] notes that this theory neglects the influence of large scale structures in the jet.

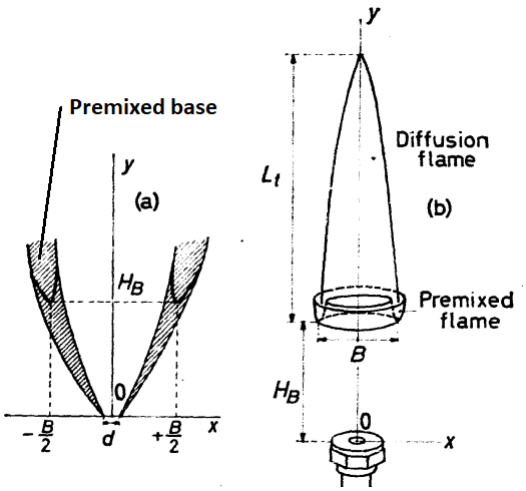

Figure 2.3: Illustration of the premixed flame theory - Left) Shaded mixing region of fuel and air with the boundaries indicating the stoichiometric condition; the premixed base - Right) Three-dimensional structure of premixed base [11]

4. **Edge flame concept**

   The flame front is stabilized as partial premixing takes place upstream of the flame edge according to Buckmaster [12]. This results in a tribrachial flame structure, a flame structure first observed by Phillips [13]. Fuel and air start to mix as soon as these exit the burner rim. This creates a partial premixed zone visualized in white in figure 2.4. One side is fuel-rich and the other side is fuel-lean, surrounding a trailing diffusion flame.

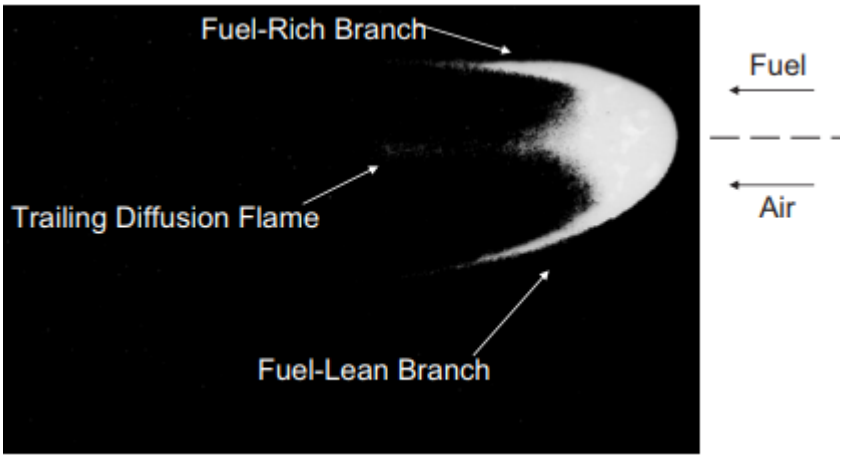

Figure 2.4: Classical tribrachial flame observed by Phillips [13] with a fuel-rich and a fuel-rich branch, followed by a diffusion flame. Adapted by Lyons [9]

5. **Large Eddy Concept**

   The large eddy concept describes the impact of large scale turbulent eddies and its induced fluid transport on flame front stabilization. The stabilization mechanism is illustrated in figure 2.5 which shows the large eddy structure carries fuel downstream to the leading edge of the flame. Meanwhile the large eddy entrains air and increases in temperature as it comes closer to the flame front. If the stoichiometric condition is reached, the structure is consumed by the flame. Lawn [8] explains the flame front propagates upstream, where the bottom part will be extinguished by strain or as it moves into the shear layer. At this point the next large eddy reaches the flame front and the described process is repeated, stabilizing the flame.

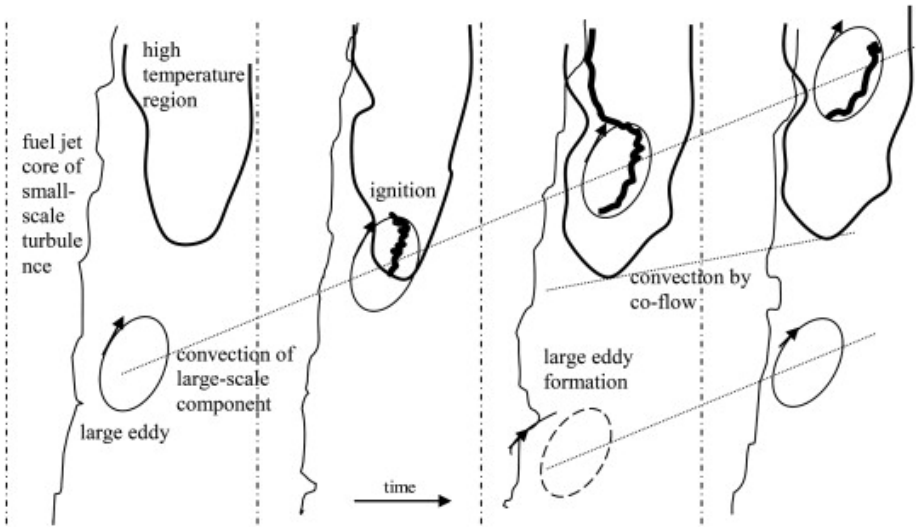

Figure 2.5: Schematic overview of the proposed large eddy stabilization mechanism in a turbulent lifted jet diffusion flame. From left to right successive time periods showing the propagation of the large eddy causing flame stabilization [8].

2.2. Lack of Clarity on Flame Stabilization Mechanism

Several theories are developed to describe the governing flame stabilization mechanisms. However, there is currently no clear consensus on the leading stabilization mechanism of the lifted turbulent jet diffusion flame. It is generally agreed on that stability of a turbulent lifted diffusion flame occurs on the edge of the flame, in which the match between the flame speed and fluid velocity stabilizing the flame, acknowledged by both Chung [14] and Lawn [8]. However, the connection of this mechanism to lift-off phenomena combined with fuel and air-stream dilution is unclear.

2.3. Flame Lift-off and Blow-out

A non-premixed jet flame can be attached to the burner rim. If the fuel and/or the coflow velocity increases the flame can lift off from the burner rim. The lifted state is attained as the stoichiometric mixture region shifts downstream with increasing fuel and/or coflow velocity. The behaviour of a specific flame can be described in flame stability charts. It maps the regions in which a flame is attached, lifted or blown-out, as function of the fuel and coflow velocity. Moore *et al.* [15] suggest blow-out happens when the local match between the flame speed and gas velocity is broken. The flame edge is moved farther downstream to a region with a too lean oxidizer-fuel mixture to sustain the flame. Dahm and Dibble [16] proposed a relation to describe the occurrence of blow-out if the ratio of a large-scale mixing time scale and a chemical time scale drops below the critical value 4.3:

$$\eta = \frac{t_{mix}}{t_{chem}} \sim \frac{\delta / u_{cl}}{\kappa / {S_L}^2} = 4.3 \tag{2.3}$$

where δ is the width of the jet and u_{cl} is the centreline velocity of the jet, κ is the thermal diffusivity and S_L the laminar flame speed. Lyons [9] mentions that the critical lift-off and re-attachment velocities are found to be subject of hysteresis. Hence there are velocity regions in which the flame can either be lifted or attached.

2.4. Impact of Hydrogen on Lifted Diffusion Flame Stability

In experimental studies by Karbasi [17], Wu *et al.* [18] and Leung and Wierzba [19] it is observed that the addition of hydrogen to a methane jet diffusion flame in a cold air coflow leads to increased flame stability. It appeared that the blowout velocity increases with higher hydrogen content of the fuel flow. In his study of a methane-hydrogen jet diffusion flame, Karbasi [17] attributes this to both enhanced mixing caused by the density difference of hydrogen and methane and to increased burning velocity of the hydrogen-methane mixture. The latter argument is also brought up by Wu *et al.* [18] in their study in which methane is added to a hydrogen fuel flow. They explain this as hydrocarbon fuels such as methane act as radical sink. The hydrocarbons consume available H, O and OH radicals quickly enough hindering the highly reactive hydrogen in its reaction. The other way around, the higher the hydrogen content in a fuel mixture, the more reactive the mixture is. Leung and Wierzba [19] studied a jet diffusion flame with a fuel mix of methane and inert CO_2 and suggest a relationship between hydrogen fuel-addition and the burning velocity. A significant increase in the blowout velocity is observed when the hydrogen concentration in the fuel flow increases. However, they note that a small amount of hydrogen does not have a large effect on the laminar flame speed. In this they refer to fundamental flame speed studies of methane-hydrogen flames by Huang *et al.* [20] and Ilbas *et al.* [21]. Leung and Wierzba [19] conclude on three aspects responsible for increasing the blow-out velocity when small amounts of hydrogen are added to the fuel. These are the strong mixing capability of hydrogen, the high thermal diffusivity leading to high ignitability of hydrogen and the capability of hydrogen to act as a radical source for the methane combustion reaction.

2.5. Impact of CO_2 on Lifted Diffusion Flame Stability

CO_2 dilution of the air coflow of lifted methane jet diffusion flames has a destabilizing effect, as widely observed both experimentally by studies of Lock *et al.* [22] and Min *et al.* [23] as numerically by a study of Guo *et al.* [24]. The latter investigation discusses the different effects of CO_2 coflow-dilution to the flame stability. The different effects are listed below.

- Chemical - altered chemical kinetics and/or chemical participation;
- Dilution - reduction in O_2 content;
- Radiation - modified radiative heat transfer;
- Thermal - change in specific heat;
- Transport phenomena - altered transport properties.

Addressing these effects, a study into the effect of coflow dilution with CO_2 on the extinction of laminar jet diffusion flames by Lock *et al.* [22] highlight the importance of the thermal, chemical and dilution effects. In a numerical investigation, Guo *et al.* [24] shows the relative importance of each effect of CO_2 dilution on the lift-off behaviour of a laminar jet diffusion flame. They observe that the most prominent effect is dilution, followed by the thermal effect whereas the chemical effect is very small. Effects of altered radiation and transport phenomena are found to be insignificant. Min *et al.* [23] experimentally confirm this in a study on the effect of CO_2 on the transition from the attached to lifted state of non-premixed jet flames in the laminar and turbulent regime. Whilst the aerodynamical impact (increased flow velocity due to CO_2 addition) is thought to have minimal effect on lift-off, the authors interpret the influence of CO_2 dilution on the lift-off height as follows: the reaction rate close to the flame edge is reduced resulting in a mismatch between flame speed and gas velocity, disrupting local flame stability. This causes the flame to stabilize more downstream, where flame and flow speed are again equal. Min *et al.* [23] cite as evidence of the reduction of

flame speed due to CO_2 addition two studies of Qiao *et al.*, a laminar premixed hydrogen-air flame [25] and a laminar premixed methane-air flame [26].

A follow-up study of Min and Baillot [27] observes the destabilizing influence of the CO_2 in the coflow on the blow-out behaviour of a lifted methane diffusion flame. Again, their findings support the conclusions of Guo *et al.* [24] on the relative importance of the effects of CO_2 dilution. Min and Baillot [27] observed increased lift-off height and fluctuations of the lift-off height at higher CO_2 concentrations. They also found that the radial stabilization point position increases with higher CO_2 content.

Elaborating on former studies of Min *et al.* [23, 27], their research group colleagues Marin and Baillot [28] indicate that there is a difference in effectiveness of CO_2 dilution of the coflow and the fuel flow, addressing the aerodynamical and dilutional effects. In case of coflow CO_2 dilution, the increased gas velocity as result of the added CO_2 and its induced mixing has a negligible effect on the flame stability and lift-off behaviour. This in contrast to diluting the fuel flow with CO_2. Furthermore they found that with increasing CO_2 diluent in the coflow, the lift-off height increases whilst the radial position remains the same. Similarly reasoned is in Min *et al.* (2010) [23], noting that CO_2 reduces the laminar flame speed due to the dilution effect. This disrupts the balance between the local flame speed and local flow speed necessary for local flame stability, forcing the flame to re-stabilize at a more downstream position.

2.6. Flow Conditions at Stabilization Point Location

Literature shows that the stability of flames is most likely governed by the edge flame concept, in which the local flame velocity matches the local gas velocity. Muñiz and Mungal [29] experimentally assessed turbulent lifted methane jet flames in air-coflow fuel-jet Reynolds numbers varying between 3800 and 22000. These flames stabilized in a low velocity region, when gas velocities ranging between approximately S_L and 3 S_L. Upatnieks *et al.* [30] experimentally assessed the flame speed and the local flow conditions at the stabilization point for two turbulent lifted methane-nitrogen jet diffusion flames (Methane-nitrogen - Re = 4300 and methane - Re = 8500). They investigated the impact of turbulence on the flame speed at the stabilization points. They report that the local turbulence intensity hardly affects the lift-off height. Moreover, the flame speed at the stabilization point does not correlate with the local turbulence intensity nor with local large eddy structures. The authors propose a stability concept in which heat released by the flame diverges the local flow upstream of the stabilization point. The local flow becomes laminar and the edge flame stability concept is applicable at the stabilization point. The low velocity zone upstream of the edge flame is visualized in figure 2.6c. In this, the flame front can be interpret as a bluff body. Muñiz and Mungal [29] expect the gas velocity to increase downstream of the stabilization point as result of thermal expansion. Gordon *et al.* [31] disagree with this theory based on PIV velocity measurements of propane and propane-argon flames with high Reynolds numbers. They do not observe divergence of the flow upstream of the stabilization point. Instead, they observe sudden jumps of the stabilization point to a more upstream position. They find different flame speeds at the stabilization point, depending on whether the stabilization point moves upstream or downstream. Therefore they condition their measured flame speed to the direction of the upstream or downstream motion of the stabilization point. Resulting mean flame speeds conditioned on upstream or downstream movement of the stabilization point are shown in table 2.1. This table also lists the results of a study by Watson *et al.* [32] of the local gas velocity at the flame base of lifted jet diffusion flames conditioned on the direction of stabilization point motion.

Paper	Year	Re	Fuel	Velocity	Downstr. $[S_L]$	#	Upstr. $[S_L]$	#
Watson *et al.* [32]	2002	4800	Methane	Flow	3.2	195	2	69
Gordon *et al.* [31]	2012	10000	75/%C_3H_8 25%Ar	Flame	1	1549	2.7	865
		15000	75/%C_3H_8 25%Ar	Flame	3	744	2.7	445

Table 2.1: Literature observations of the mean flow and flame velocities at the stabilization point conditioned to its upstream and downstream motion. The mean flame speed is non-dimensionalized by the laminar flame speed S_L. The symbol # marks the number of samples per observation.

Joedicke *et al.* [33] report on the flame stabilization of lifted methane jet diffusion flames with fuel jet Reynolds numbers between 3080 and 8280. They suggest that flame stability is guaranteed if the local turbulent flame speed matches with the local gas velocity at the stabilization point. Moreover, they observe flow velocities at the stabilization point similar to those found by Upatnieks *et al.* [30]. They state that flame stability is garantueed if the local laminar flame speed equals the local gas velocity, in contrast to what is reported by Joedicke *et al.* [33]. Unlike what Upatnieks *et al.* [30] suggest for lifted methane jet flames, Tacke *et al.* [34] report the strong influence of turbulence structures on flame stability at the stabilization point, in their study of pure-hydrogen and hydrogen-nitrogen fuels in high Reynolds environment ($17000 \leq Re \leq 40000$). This view is shared by Oh and Yoon [35] who conducted experiments in turbulent lifted hydrogen air-coflow flames. They suggest stabilization occurs in a low velocity mixing region wherein the gas velocity matches the turbulent flame speed. In his review paper, Lawn [8] states that the gas velocity at the stabilization point is generally found to be higher than the laminar flame speed. Furthermore, the gas velocity is found to be lower than expected if it is based on turbulent flame stabilization theories. This is illustrated in table 2.2, listing the mean flame speeds observed in measurements of Su *et al.* [36] and Upatnieks *et al.* [30], including the upper and lower limits.

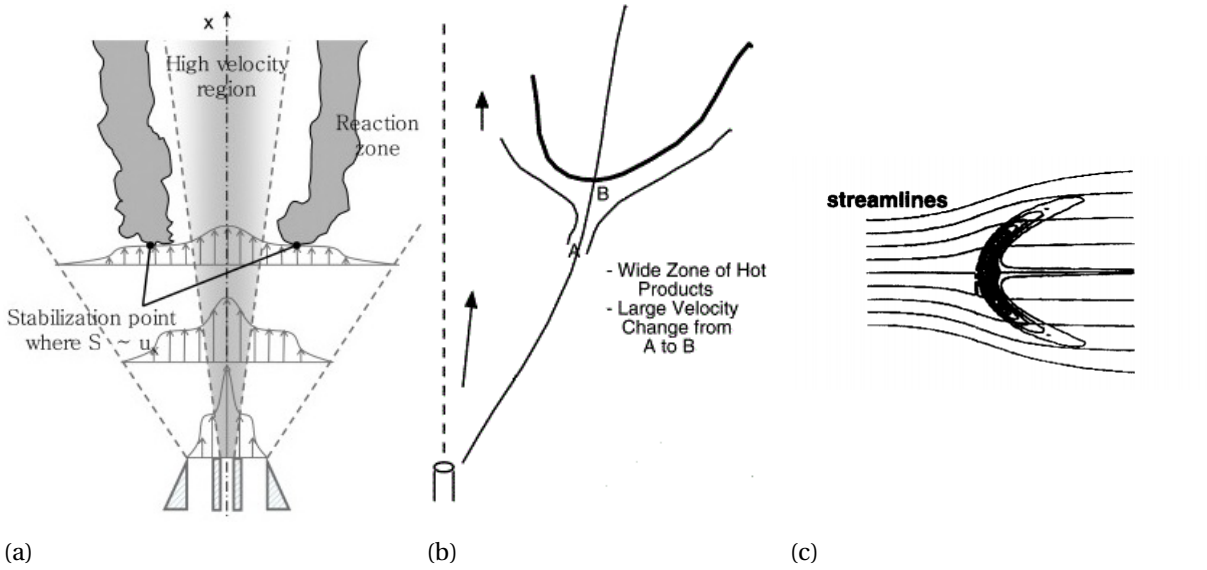

(a) (b) (c)

Figure 2.6: Schematic overview clarifying a possible low-speed region upstream the stabilization point: a) Stabilization points in theoretical turbulent jet in air-coflow flame, adapted from [35]. b) Schematic of the right-hand-side flame base plotted along with the stoichiometric contour crossing the flame base. The two streamlines starting in A divert around the flame base, resulting in a large decrease of gas velocity from point A to B. Adapted from [30]. c) Zoom-in on the edge flame resembling a triple flame, plotted along with diverging streamlines around the triple flame, adapted from [29]

Paper	Year	Re	Fuel	Mean	Min	Max	#
				$[S_L]$	$[S_L]$	$[S_L]$	
Su *et al.* [36]	2006	4400	Methane	1.8	-1	4	88
Upatnieks *et al.* [30]	2002	4200	Methane	0.7	-1	2.3	1097
		8500	Methane	1.2	-4	7.9	2012

Table 2.2: Literature observations of the flame speed at the stabilization point. Listed are the mean, minimum and maximum values of flame speed non-dimensionalized by the laminar flame speed S_L. # denotes the number of samples per observation.

2.7. Flammability Conditions at Stabilization Point Location

Su *et al.* [36] reject the assumption that lifted jet diffusion flames stabilize on the most upstream point of the flame edge, based on research of lifted methane jet flames with Reynolds number ranging between 4400 and 10700. They suggest that the mean fuel-oxidizer mixture at the most upstream point of the flame edge is too lean for combustion. Instead a position more to the centreline of the fuel jet is proposed as stabilization point location. Joedicke *et al.* [33] share this view, stating that the stabilization point is located in the fuel-rich region where the mixture fraction is 10% above the stoichiometric mixture fraction. Lawn [8] suggests fuel is irregularly transported towards the flame base by intermittent turbulent eddies. This enables combustion to take place even though the mean mixture concentration is too lean. This discussion is different for hydrogen flames, whereas Tacke *et al.* [34] suggest that the stabilization point is identified in fuel-lean regions and its location being indifferent to the local mixture fraction. Oh and Yoon [35] suggest that the respective stabilization point is located in the mixing region.

2.8. Research Potential in Lifted Diffusion Flame Stability Influenced by Hydrogen and CO_2 at the Stabilization Point

The stabilization mechanism(s) of a turbulent lifted jet is not fully understood. Research questions remain open despite the fact that a lot of attention is paid to flow and flammability conditions at the stabilization point of pure hydrocarbon flames. Many stabilization theories are proposed, but open questions remain on the effect of several relevant quantities at the stabilization point on flame stability, namely the local turbulence intensity, the local mixture fraction, the local flame and the local gas velocity on stability. Literature also reports on the effects of hydrogen fuel-addition and CO_2 coflow-dilution on lift-off and blow-out behaviour of the turbulent lifted jet. Nonetheless, the effect of hydrogen fuel-addition on flame stabilization aspects as flame speed and flow conditions at the stabilization point is poorly understood. Moreover, current state of research is mainly focused on the effect of sole fuel-side hydrogen addition or sole coflow-side CO_2 dilution on turbulent lifted diffusion flame stability.

3

Experimental Setup

3.1. The DJHC Burner

The Delft-Jet-in-Hot-Coflow burner, abbreviated as the DJHC buner, is used by the Delft Process & Energy group to study jet flames issuing in a coflow of vitiated air. The design of the DJHC burner is based on the Jet-in-Hot-Coflow burner of the combustion research group of the University of Adelaide [37]. Compared to the latter, the DJHC is suited for PIV and/or LDA measurements as it allows seeding of the coflow and fuel flows with tracer particles. It was formerly used to study certain aspects of flameless oxidation such as the mixing of fuel and vitiated air prior to combustion. In the current investigation, the same burner is used in research towards combustion with cold exhaust gas recirculation and hydrogen fuel-addition. The setup allows for air-side dilution with inert species such as CO_2 and N_2 and fuel-side addition of hydrogen to the main fuel which is Dutch natural gas (DNG).

Figure 3.1 shows the layout of the burner including a zoom-in on the geometry of the top of the burner. The burner comprises of fuel and oxidizer inlets and piping, flow distribution rings and plate inserts ensuring homogeneous flow inside the burner annulus and a partially premixed ring burner to heat the coflow. The fuel exits the fuel pipe which has a 4.5 mm internal diameter. In cold condition, the burner tip is 15 mm above the outer pipe-exit of the burner, which has an outer diameter of 89.2 mm with a wall thickness of 3.2 mm. Figure 3.1 also shows the coordinate system that is used in this study. Its origin is at the centre of the fuel pipe exit, with an upwards positive axial component, z, and east-orientated positive radial component r, see figure 3.1 for details.

The mass flows of the species making up the fuel and coflow are user-defined in a Labview environment. This dictates the four Bronkhorst mass flow controllers of type EL-FLOW responsible for controlling the inflow of four species, namely for DNG, hydrogen, air and CO_2. The mass flow controllers have an inaccuracy of 5% of the reading plus 0.1% of the full scale. The fuel and coflow exit the burner at ambient conditions of the laboratory, namely 1.023 bar and 300 K.

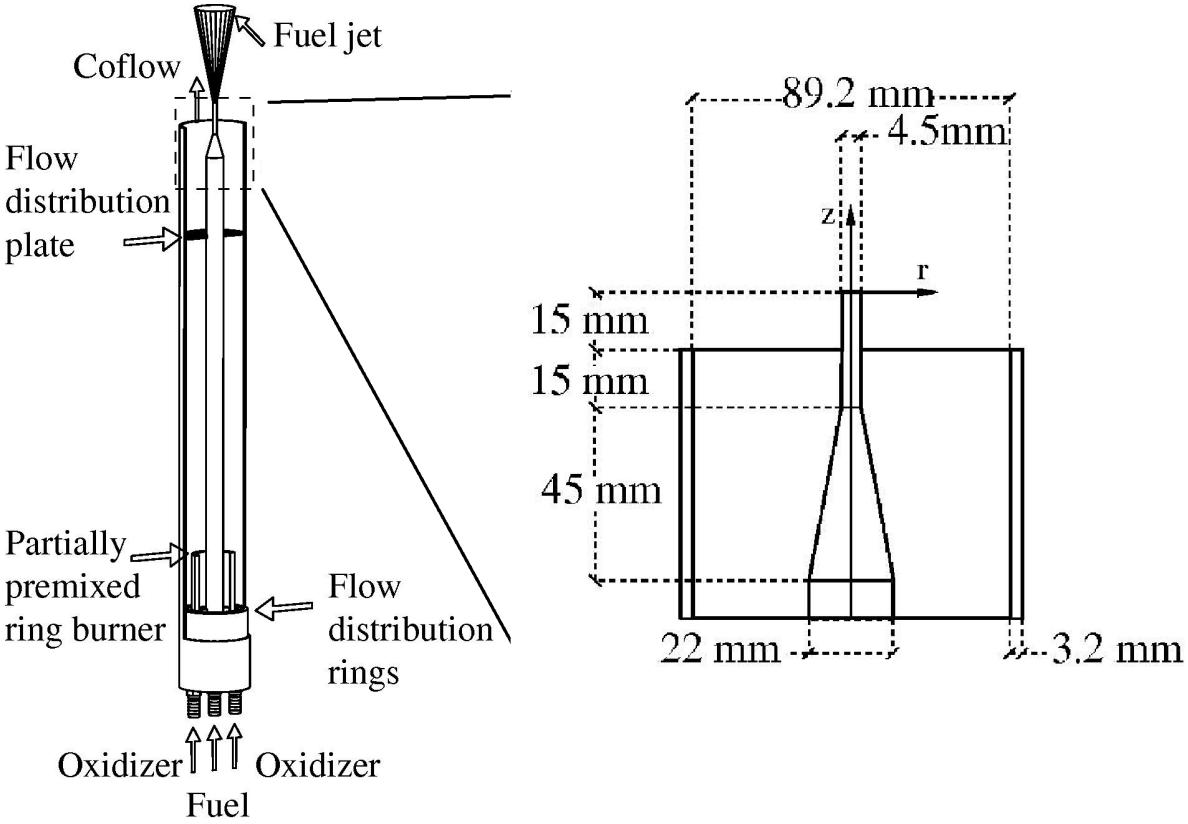

Figure 3.1: Schematic overview of the Delft Jet-in-Hot-Coflow burner with zoom-in on burner exit, adapted from [38].

3.2. OH* Chemiluminescence

Flame chemiluminescence is based on photographically capturing the photons emitted by excited OH radicals (OH*) in the combustion reaction zone. During the combustion reaction, a chemical pathway is followed where OH radicals are formed in the high temperature reaction zones. As part of this chemical pathway the OH radicals are excited and release a photon, indicating the combustion reaction zone. It is important to note that recording OH* luminescence with a camera is a line-of-sight measurement technique. This means that the observed signal is the summation of photons emitted over the line-of-sight.

OH* images are taken with a Optronis Camrecord 600 camera equipped with a Lambert Instruments fiber-optically coupled intensifier type HI-CAM CR. The light emitted by the OH* radicals is collected by a Nikon 1:4.5 UV-Nikkor lens with focal length of 105 mm. This lens is able to collect light in the 220-900 nm wavelength range and is fitted with a ThorLabs 308 nm bandpass filter with 20 nm full-width at half maximum. This as the relevant wavelength of the emitted light is in between 306 nm and 310 nm. Therefore, the camera sensor only captures the OH* luminescence. HiCam CR V3.4 software is used to synchronize the intensifier with the 400 μs exposure time of the camera. The intensifier gain is set on 3×10^3. The intensified light is then collected on the sensor of the camera forming an image of 512x1280 pixels and is then stored on the camera memory. The resolution is 7.9 pixels per millimeter, resulting in a field-of-view with a size of 65 x 162 mm^2. Optronis CamControl software is used to control the camera and transfer the images from the internal storage of the camera to an external storage device for later processing of the data. Per flame 5000 images are taken at a rate of 50 Hz.

3.3. Particle Image Velocimetry

Particle image velocimetry (PIV) was used to obtain statistical information on the stabilization point location and the local flow conditions at this point. In contrast to the OH* luminescence, PIV is a planar measurement technique meaning the flame is solely assessed in a two-dimensional cross section of the flame.

The PIV system used in this study comprises of a Quantronix Nd:YLF dual-cavity laser system type Darwin-Duo Pro 527-80-M. In this laser system the output of two ND:YLF lasers are combined in one output beam using internal optics. The 527 nm laser beam emitted by the laser system is transformed into a 150 mm high laser sheet with a thickness of approximately 1 mm by using three successive lenses. The burner height is adjustable depending on the flame case. Alumina-oxide particles of 1μm in diameter are used as seeding. To prevent coagulation of particles, an anti-coagulant agent is mixed with the seeding particles and the mixture is dried prior to use in an oven at 473 K for approximately 4 hours. Two cyclone seeders are used to disperse the seeding; one dedicated to the fuel flow and the other to the coflow. The light scattered by the seeding particles is recorded by a Fastcam SA1.1 camera equipped with a Nikon micro nikkor 1:2.5 lens with focal length of 60 mm. The lens is equipped with a 532 nm bandpass filter with 10 nm full-width at half maximum. A LaVision pulse delay generator ensures synchronization between the laser and camera. The entire PIV system is operated through the acquisition module of the DaVis 8.4 software.

The first image of the image pair is shot taken at time t and the second at time $t + \Delta t$ with a Δt = 150μs. With an image of 1024x2024 pixels, a spatial resolution of 6.35 pixels per millimeter is achieved. This results in a 161mm x 161 mm sized field-of-view. PIV recordings are done at the same moment as the OH* recordings to ensure both measurement systems capture the time resolved statistics of the flame correctly. The image processing module of the DaVis 8.4 software performs the PIV algorithm to yield velocity fields. In this algorithm, three passes are done over a 32 x 32 pixels interrogation area with 50% overlap followed by 4 passes over a 16 x 16 pixels interrogation area with 50% overlap. A median filter is locally applied if a velocity vector deviates more than two standard deviations from the mean of the local velocity vector. Per flame 5000 image-pairs are taken at a rate of 50 Hz and 2.5 kHz to resolve for the stabilization point location and the rapid motion of the stabilization point, respectively.

3.4. Description of the Flame Cases

The investigated flames use Dutch Natural Gas (DNG) and hydrogen as fuel and the oxidizer flow consists of air and CO_2. DNG is a mixture of methane, nitrogen, ethane and a minor fraction of mainly other hydrocarbons [39]. The composition of DNG is given in table 3.1. This table describes the composition (mole fraction) of the different fuels and coflows that are considered in this study. Four flames are defined in which hydrogen increasingly replaces the fraction of DNG without adding CO_2 to the coflow to assess the impact of hydrogen on flame stability. To investigate the effects of CO_2 dilution of the coflow of DNG/hydrogen flames, two flames with 25% hydrogen in the fuel have a nonzero CO_2 fraction in the coflow. In this report, the different flames will be named after their fractions hydrogen and CO_2 while the flame operating on pure DNG and air will be referred to as "DNG".

Flame	DNG 0% CO_2	5% H_2 0% CO_2	10% H_2 0% CO_2	25% H_2 0% CO_2	25% H_2 4% CO_2	25% H_2 8% CO_2
	Fuel Composition x_i [-]					
CH_4	0.813	0.772	0.732	0.61	0.61	0.61
N_2	0.144	0.137	0.13	0.108	0.108	0.108
C_2H_6	0.037	0.035	0.033	0.028	0.028	0.028
H_2	0.000	0.05	0.1	0.25	0.25	0.25
Rest	0.006	0.006	0.005	0.005	0.005	0.005
	Coflow Composition x_i [-]					
O_2	0.21	0.21	0.21	0.21	0.2016	0.1932
N_2	0.79	0.79	0.79	0.79	0.76	0.73
CO_2	0	0	0	0	0.04	0.08

Table 3.1: Composition (in mole fraction) of the fuel and coflow of the investigated flames.

The proportions hydrogen and DNG are chosen identical to the proportions considered in Arteaga Mendez *et al.* [38], wherein lifted diffusion hydrogen-methane flames in a vitiated coflow environment are studied. Table 3.2 lists the flow rates in normal liters per minute (nl/min) set by the mass flow controllers with corresponding uncertainties in nl/min for each of the flames considered in this investigation. The temperature and pressure of the flows are taken as 300 K and 1.023 bar. To be consistent with the approach in Arteaga Mendez *et al.* [38], the fuel flow rates are chosen to maintain a near constant fuel-jet Reynolds number. The flow rates of the coflow are selected to set the bulk velocity at 0.51 m/s in all flame cases.

Flame	DNG 0% CO_2	5% H_2 0% CO_2	10% H_2 0% CO_2	25% H_2 0% CO_2	25% H_2 4% CO_2	25% H_2 8% CO_2
	Fuel Flow Rate [nl/min]					
DNG	18.45	18.24	18.11	17.28	17.28	17.28
Uncertainty	0.142	0.141	0.141	0.136	0.136	0.136
H_2	0	0.96	2.01	5.77	5.77	5.77
Uncertainty	0	0.030	0.035	0.054	0.054	0.054
	Coflow Flow Rate [nl/min]					
Air	150	150	150	150	144.0	138.0
Uncertainty	1.25	1.25	1.25	1.25	1.22	1.19
CO_2	0	0	0	0	6	12
Uncertainty	0	0	0	0	0.09	0.12

Table 3.2: Mass flow rates of coflow and fuel flow (with corresponding uncertainties).

Table 3.3 lists some relevant properties of the studied flames, the Reynolds number of the fuel jet, the bulk velocity of the fuel, the mass flow rate of the fuel, the power output of the flame, the stoichiometric mixture fraction, the laminar flame speed and the adiabatic flame temperature of the flame. In deriving some of these values the validity of the ideal gas law is assumed. The density, dynamic viscosity and lower heating value of the fuel mixtures are extracted from Refprop 9.0 [40]. The stoichiometric mixture fraction, laminar flame speed and adiabatic flame temperature are determined with CHEM1D [41] as a 1D free-propagating laminar flame. One should note in extracting these values from the software, the fraction "rest" in table 3.1 is normalized to the mixture

fractions of methane and ethane. This is for the reason that the fraction "rest" mainly consists of hydrocarbons.

Flame	CO_2 [%]	Re_{fuel} [-]	u_{fuel} [m/s]	$\dot{m}_{fuel}$ [g/s]	P [kW]	S_L [m/s]	Z_{st} [-]	T_{ad} [K]
DNG	0	6004	21.0	2.51	9.8	0.371	0.0699	2204
5% H_2	0	5992	21.9	2.50	9.8	0.385	0.0693	2207
10% H_2	0	6003	22.9	2.50	9.9	0.400	0.0687	2210
25% H_2	0	5923	26.3	2.44	10.2	0.457	0.0665	2220
25% H_2	4	5923	26.3	2.44	10.2	0.355	0.0627	2141
25% H_2	8	5923	26.3	2.44	10.2	0.274	0.0591	2064

Table 3.3: Flame properties of the investigated flames. Re_fuel is the Reynolds number of fuel jet, u_{fuel} is the bulk velocity of the fuel-jet (in m/s), $\dot{m}_{fuel}$ is the mass flow rate of the fuel (in g/s), P is the power output of the flame (in kW), S_L is the laminar flame speed (in m/s), Z_{st} is the stoichiometric mixture fraction and T_{ad} is the adiabatic flame temperature in K.

4

Results concerning the Methodology

4.1. Extraction of Lift-off Height from OH* Images

The lift-off height is extracted from the instantaneous OH chemiluminescence (OH*) images. A dark image is subtracted from every OH* image for calibration, this results in figure 4.1a. First a dark image is constructed by averaging 100 images taken with the lens cap on. The dark image is subtracted from each individual OH* image. For one arbitrary chosen OH* image the result is shown in figure 4.1. To increase the contrast, contrast stretching is applied leaving out the lower 1% and upper 95% of the pixel values, yielding figure 4.1b. To remove noise, each image is then filtered by an averaging disk with a radius of 8 pixels, producing figure 4.1c. The image is subsequently binarized after which the flame boundary is detected. The vertical coordinate of the lowest point of the flame boundary yields the lift-off height and is marked with a red cross in figure 4.1d. The lift-off height extraction process is fully automated, as all the OH* images are processed by a Matlab routine.

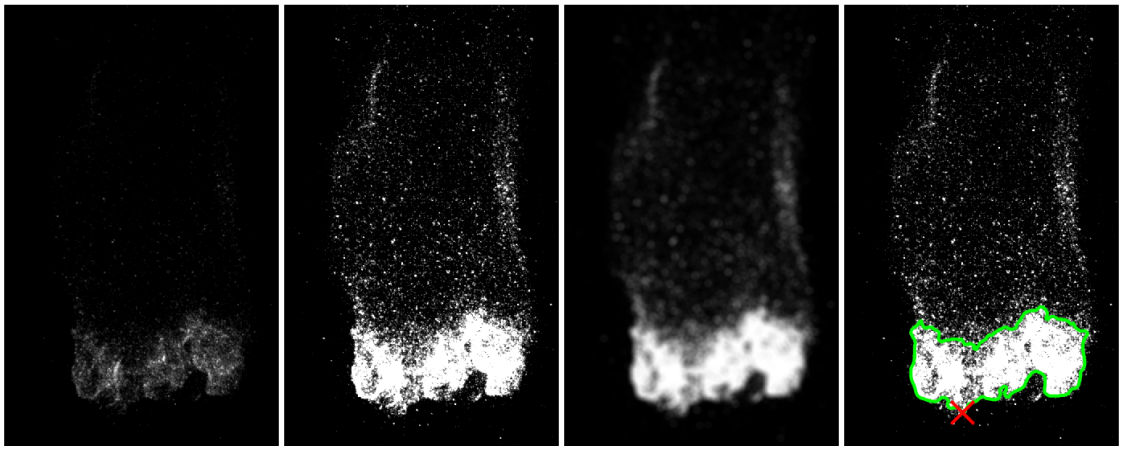

(a) (b) (c) (d)

Figure 4.1: Different steps in the procedure to extract the lift-off height from OH* images.a) OH* image with dark image substracted b) Contrast stretched image d) Scaled image with resulting flame boundary and lift-off height location.

4.2. Extraction of Stabilization Point Location from PIV Images

The Matlab routine has to extract the stabilization point from the raw PIV image, showing the seeding particles when illuminated by the laser light in a planar cross section of the flame. The combustion product in the flame region have a much higher temperature compared to the unburned gas, leading to lower seeding density in the burned gas region. The boundary between the hot and cold gas can be clearly observed from the images by a sudden change in the seeding density. Hence, the seeding quality in the PIV image is key to the accurate extraction of the stabilization point location. Figure 4.2a shows an ideal seeding profile. One can clearly observe two concave low seeding density regions representing the hot combustion gases with the reaction zone at the base. The lowest point of these two regions is considered the stabilization point location.

A Matlab processing routine is developed to accurately extract the stabilization point location. Figure 4.2 illustrates the procedure to find the stabilization point location for a randomly chosen PIV image of a 10% H2-90% DNG flame. Figure 4.2a shows a raw PIV image of which the contrast is stretched by leaving out the lower and upper 1% pixel values. The image is filtered by a Gaussian filter with a square kernel with standard deviation of 8 pixels to reduce noise as is visible in figure 4.2b. The contrast of borders between low and high pixel value areas is enhanced by unsharp masking with a 20 pixel radius Gaussian filter as in figure 4.2c. Unsharp masking is an image processing operation in which the filtered version of the image is subtracted from the original image yielding an sharpened version which improves the accuracy of the binarization in the next step. This image is then binarized and the edge is determined describing the flame boundary. The stabilization point is the lowest point on the boundary describing the low density concave areas. Figure 4.2d shows the final PIV image with the described boundary in green and the stabilization point is marked by a red cross.

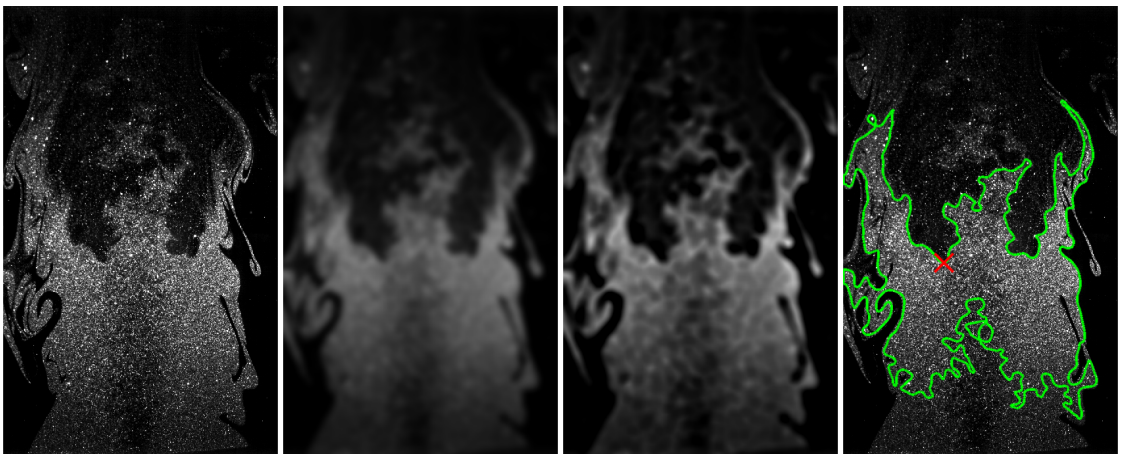

(a) (b) (c) (d)

Figure 4.2: Different steps in the procedure to extract the stabilization point from PIV images. a) PIV image after contrast stretching. b) PIV image result after filtering. c) PIV image after unsharp masking. d) Scaled image with detected flame boundary and stabilization point.

The stabilization point locations are extracted from the raw PIV images, in a partly automatized procedure as manual extraction is highly time consuming for large number of images. Figure 4.3 illustrates the protocol that is developed to analyze large number of images. The PIV images are automatically assessed by the Matlab processing routine that extracts the stabilization point from the image. If the Matlab routine is unable to extract the stabilization point from an image, it is flagged for manual stabilization point extraction. All images in which Matlab found a stabilization point are manually checked to ensure correct extraction. If the stabilization point location found by Matlab is rejected than it will be extracted manually. If it is impossible to determine the stabilization point in the manual extraction step the image is discarded.

The procedure combines the best of both automatic and manual image extraction. Automatic stabilization point detection is highly time efficient but can yield erroneous stabilization point locations. This occurs when images have a too low seeding particle density to clearly visualize the stabilization point location. In that case, manual extraction yields stabilization points from most of these images.

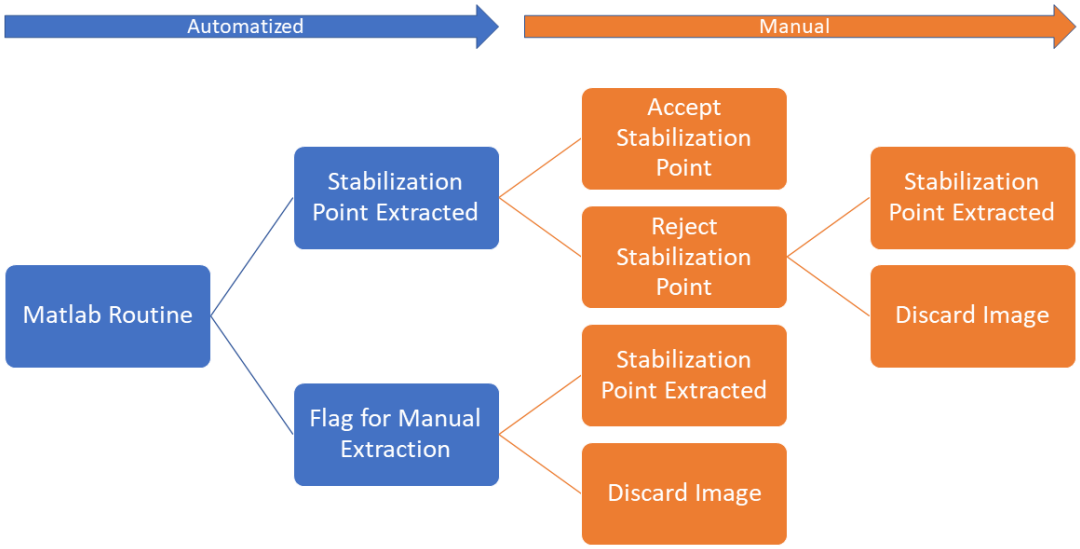

Figure 4.3: Stabilization point location extraction protocol. Blue indicates the automatized steps and orange the manual steps.

4.3. Stabilization Point Trajectories

High frequency (2.5 kHz) PIV measurements were performed to determine the trajectories of the stabilization point and the local flame speeds. The extraction is performed according to the protocol depicted in figure 4.4 using the same Matlab processing routine as described in section 4.2. Visual inspection assesses all the stabilization point locations determined by the Matlab routine but unlike in the former procedure, no subsequent manual extraction of the stabilization point takes place. This is as the error in manual extraction is relatively large compared to the stabilization point displacement in consecutive PIV images in high frequency PIV measurements.

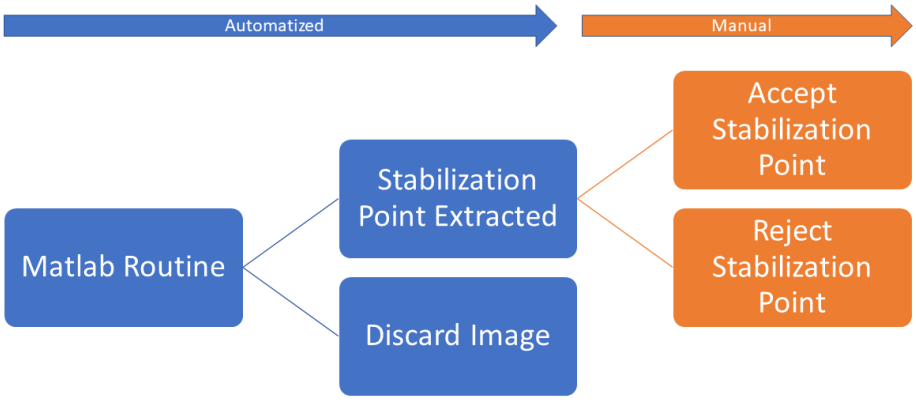

Figure 4.4: Stabilization point location extraction protocol for the time resolved PIV measurements. Blue indicates the automatized steps and orange the manual steps.

A sequence of consecutive stabilization point locations forms a trajectory. The start of a trajectory is indicated by a large displacement in stabilization point location (jump). The definition of a jump is dynamically defined per flame as the 95 percentile of the absolute displacements of the collected stabilization point locations. Only trajectories consisting of at least 5 stabilization points are considered, ensuring that the correct transient behaviour of the stabilization point is captured.

4.4. Stabilization Point Velocity and Gas Velocity

The stabilization point velocity u_{stab} is calculated by numerically differentiating the axial stabilization point locations with respect to time using a finite difference scheme. A brief sensitivity study is done to asses the different numerical schemes. The results are shown in figure 4.5. The axial displacement of the stabilization points forming a typical trajectory of a DNG flame are taken and three finite difference methods are applied, forward difference, central difference, and a five-point stencil as in

$$u_{stab_i} = \left(\frac{\Delta z}{\Delta y}\right)_i \approx \frac{z_{i-2} - 8z_{i-1} + 8z_{i+1} - z_{i+2}}{12\Delta t}, \tag{4.1}$$

where z_i is axial position of the stabilization point at element i in the trajectory and Δt the timestep which equals $\Delta t = 1/2500$ s.

It can be concluded that the influence of the numerical schemes is limited. The five-point-stencil is preferred over the forward-difference method and the central difference method, as the former produces smoothen results. This choice is consistent with the approach of Upatnieks *et al.* [30] in similar research.

The gas velocity u_{piv} is extracted from the instantaneous PIV velocity fields, at a location just upstream of the stabilization point in such a way that the interrogation area is fully in the unburned gas region. Three PIV vectors are assessed, namely of the interrogation area overlapping the stabilization point and respectively one and two interrogation areas upstream the stabilization point. As each PIV vector covers 8 x 8 pixels with a spatial resolution of 6.35 mm/pixel, this yields the PIV vector 0, 1.25 and 2.5 mm upstream of the stabilization point respectively. The bottom plot of figure 4.5 shows the result. No significant differences are visible, but the 0 mm option is undesirable as its interrogation area possibly overlaps with the burned gas region. In this view, the option to extract data from the vector containing velocity data from the interrogation area 1.25 mm upstream is considered sufficient. This as is expected an interrogation area more upstream as the 2.5 mm option, would lose valuable information about the flow locally at the stabilization point. This consideration is in accordance with similar research of Gordon *et al.* [31].

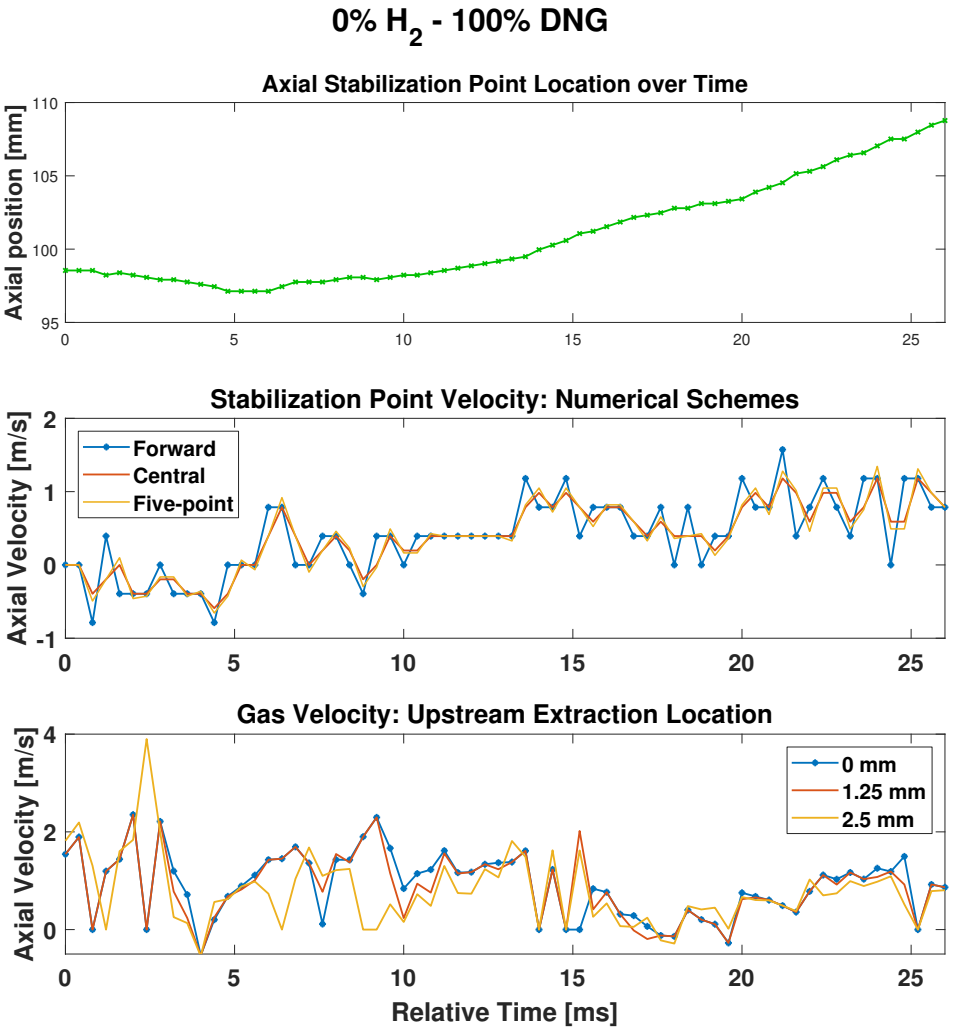

Figure 4.5: Sensitivity studies assessing the numerical schemes for the stabilization point velocity and the extraction point location for the gas velocity. Top) Axial position of typical trajectory of DNG flame. Middle) Axial stabilization point velocity derived from typical trajectory through the forward, central and five-point-difference method. Bottom) gas velocity from corresponding PIV calculations of the typical trajectory, for three upstream extraction locations upstream of the stabilization point.

4.5. Burning Velocity

From this point, the definition of burning velocity is chosen to accurately represent the velocity of the flame front relative to the unburned fuel-oxidizer mixture. The burning velocity is computed from the stabilization point velocity u_{stab} and the reactant gas velocity u_{PIV} just below the stabilization point, both in axial direction. The burning velocity u_{burn} is then defined as the difference in gas velocity u_{PIV} and the stabilization point velocity u_{stab}

$$u_{burn} = u_{PIV} - u_{stab}. \tag{4.2}$$

The gas velocity u_{PIV} and the stabilization point velocity u_{stab} are taken positive in positive z-direction (upwards), whereas the burning velocity u_{burn} is taken positive in the negative axial direction (downwards). Figure 4.6 illustrated this.

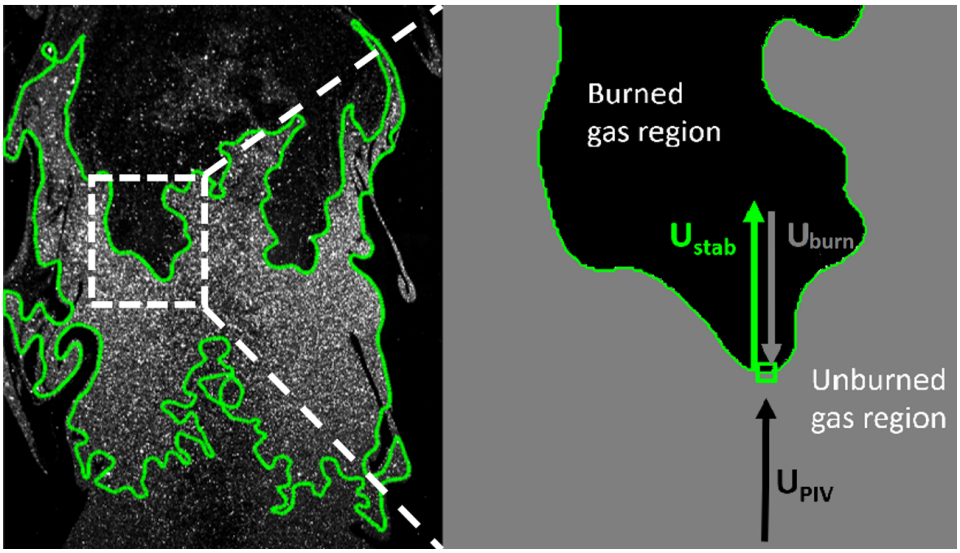

Figure 4.6: Schematic of coordinate system in calculating the burning velocity u_{fl}, derived by subtracting the stabilization point velocity u_{stab} from the gas velocity u_{PIV} upstream of the stabilization point. The gas velocity u_{PIV} and the stabilization point velocity u_{stab} are taken positive in positive z-direction (upwards), whereas the burning velocity u_{burn} is taken positive in the negative axial direction (downwards).

5

Results and Discussion

5.1. Effect of Hydrogen on Flame Stabilization

5.1.1. Lift-off Height and Stabilization Point Location

The effect of hydrogen addition on flame stabilization is investigated by assessing the 0%, 5%, 10% and 25% hydrogen flames without CO_2 dilution of the coflow. The Reynolds number is approximately the same for these flames i.e. Re_{fuel}, see table 3.3 at page 15.

Figure 5.1 shows a scatter plot of the lift-off height extracted from the OH* images (blue markers) and the stabilization point locations extracted from the PIV images (red markers) of the investigated flames. Furthermore the half-width line of a typical turbulent jet is plotted, describing the radial position where the mean velocity equals half of the centreline velocity of the jet. This is to get preliminary insight in the gas velocity of the region where the flame stabilizes. The line also describes the spreading of a typical jet. The radial position is described as

$$r_{1/2} = 0.0965(z - z_0) \tag{5.1}$$

where z is the axial position, $z_0 = -6.8\frac{z}{D}$ the virtual origin and D is the diameter of the fuel jet nozzle [42].

Figure 5.1 shows that the distribution of the data points resemble the spread of a typical jet, regardless of the hydrogen content. The bulk of the stabilization points are located outside of the theoretical jet-half-width line, indicating that the flame stabilizes in a low-velocity region. This suggestion is strengthened by a similar deduction by Muñiz and Mungal [29] in a study of turbulent lifted methane jet diffusion flames.

Furthermore, figure 5.1 shows that the lift-off height and stabilization point location shift upstream with increased hydrogen content of the fuel. The reduced lift-off height and the upstream shift of the stabilization point is likely due to the increased burning velocity when the hydrogen concentration in the fuel is increased. This has also been observed by Karbasi [17] and Wu *et al.* [18] for lifted hydrogen-methane jet diffusion flames. In the current investigation, the laminar flame speed increases with 23% when going from the pure DNG flame to the 25% H_2 flame. Hence, the hydrogen flames are able to stabilize at more upstream positions where the local gas velocity is higher. Nonetheless, from table 3.3 it becomes clear that the burning velocity of the DNG-hydrogen mixture does not increase proportionally to the hydrogen content to the laminar flame speed of a pure hydrogen flame of 2.28 m/s as extracted from CHEM1D [41]. Even though, the flames with small fractions of hydrogen in the fuel mixture, i.e. the 5% and 10% hydrogen flames, do show increased flame stability.

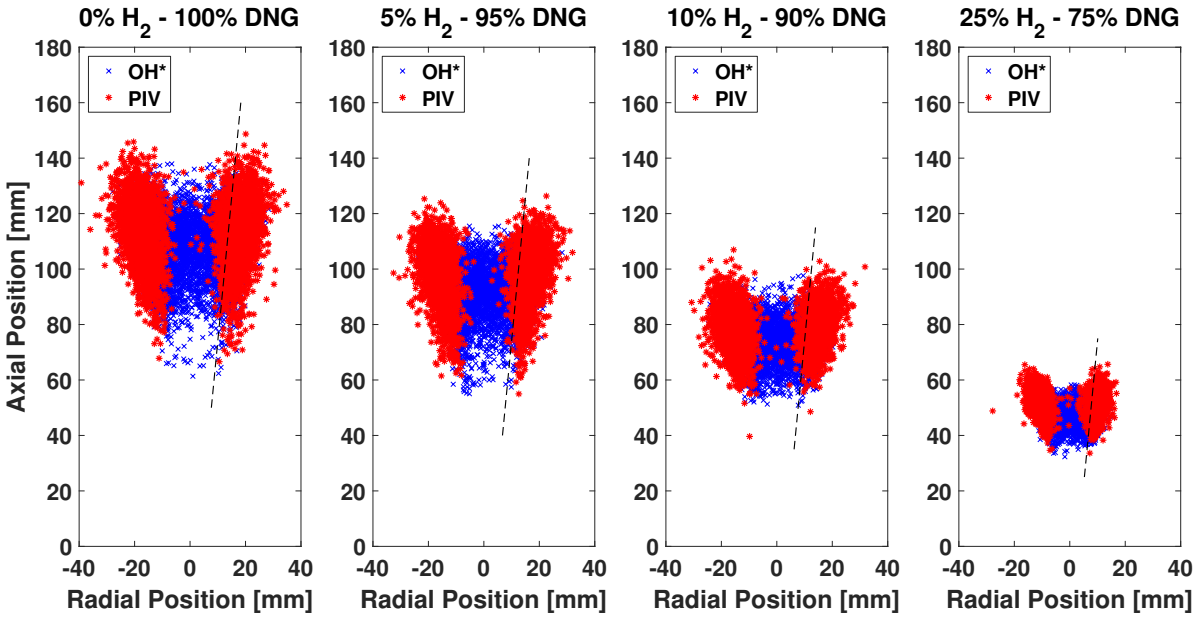

Figure 5.1: Scatter plots of lift-off heights extracted from OH* images (in blue) and stabilization point locations extracted from PIV images (in red) for the DNG and hydrogen flame cases. The dashed line represents the jet-half-width.

Yet, hypothesis is that other aspects associated to hydrogen account for this. The high thermal diffusivity of hydrogen makes the fuel-oxidizer mixture increasingly flammable with higher hydrogen fraction. Table 3.3 shows that the adiabatic flame temperature increase with increasing hydrogen content of the fuel. This illustrates that with increasing hydrogen in the fuel, the combustion becomes energetically more intense. This as hydrogen supplies radicals for the oxidation reaction of methane intensifying the combustion reaction. In addition, the mixing capability fuel-oxidizer mixture is enhanced due to the high mass diffusivity of hydrogen. Therefore it is expected that the stoichiometric conditions are more towards the jet-centre. This shift is also reached due to the high combustion reactivity of hydrogen, as the stoichiometric mixture fraction reduces with increasing hydrogen content.

Figure 5.2 shows the PDFs of the lift-off height and to the axial position of the stabilization point (left). It is seen that there are discrepancies between the lift-off height and the axial stabilization point location. The downstream tails of the PDFs of the lift-off height and the axial stabilization point location do not overlap, whereas the upstream tail of the axial stabilization point location reaches higher values than the tail of the lift-off height. This as OH* and PIV measurements probe a three-dimensional flame differently, namely along a line-of-sight and in a planar cross section, respectively. Therefore the lift-off height represents the most upstream point integrated over the entire depth of the flame, whereas the axial stabilization point location captures the most upstream point in the fixed planar cross section though the flame. This plane does not always contain the most upstream point of the entire flame. For this reason the stabilization points extracted from the PIV images do not necessarily represent the stabilization points of the entire flame. However, the most upstream point of the flame does occasionally occur in the illuminated plane, and so the most upstream values of the lift-off height and axial stabilization point location are expected at the same height.

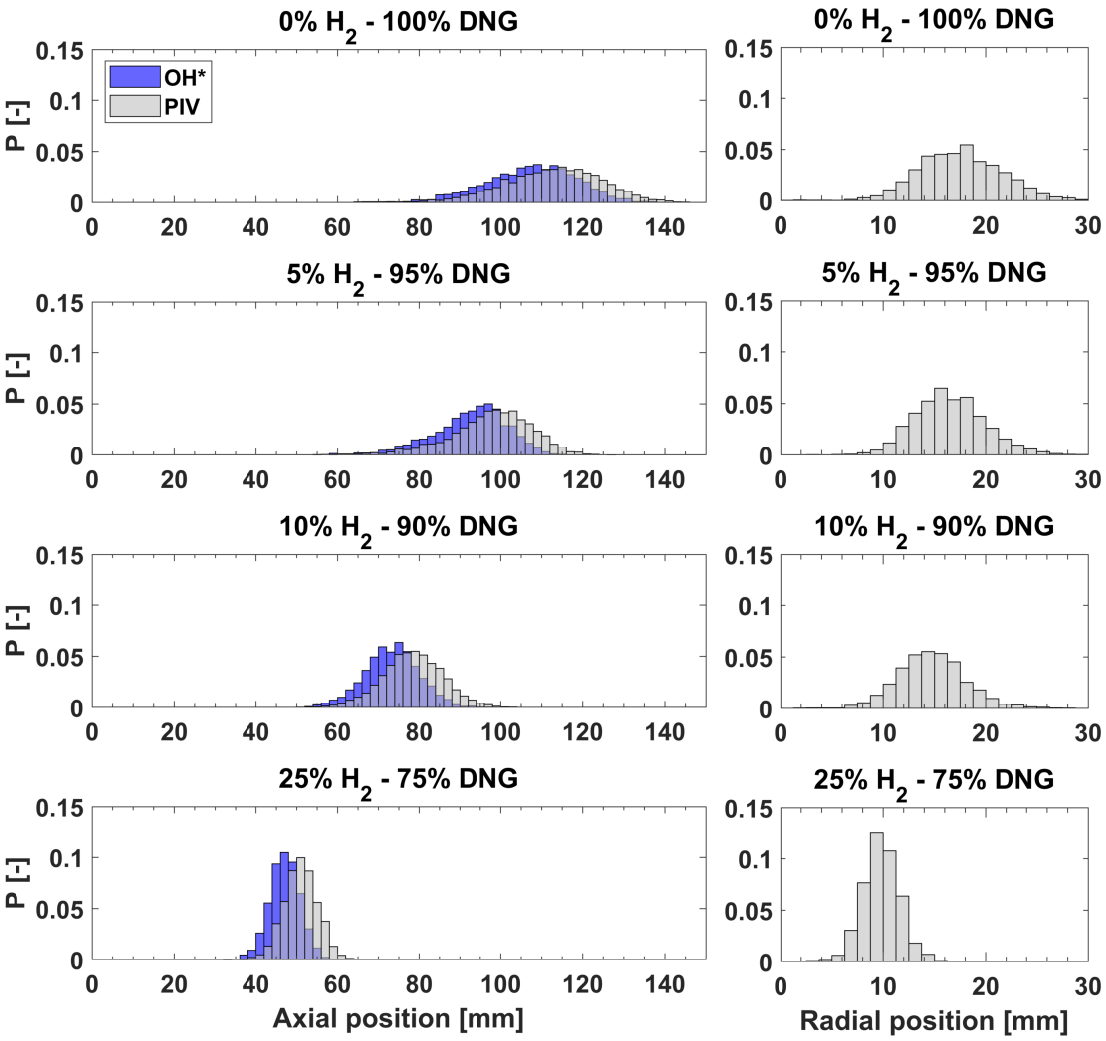

Figure 5.2: Left) PDFs of the lift-off height (blue) and the axial stabilization point location (grey). Right) PDFs of radial stabilization point location.

		OH* Axial		PIV Axial		PIV Radial	
Flame		μ [mm]	σ [mm]	μ [mm]	σ [mm]	μ [mm]	σ [mm]
0% H_2	100% DNG	107.3	11.3	112.6	11.9	17.6	4.1
5% H_2	95% DNG	92.4	9.4	97.6	10	16.5	3.5
10% H_2	90% DNG	73.3	6.7	78.4	7.4	14.8	3.4
25% H_2	75% DNG	47.1	3.7	51	4.1	9.8	1.8

Table 5.1: Values of the mean and standard deviation of the PDFs in figure 5.2.

The PDFs on the right column of figure 5.2 show that the radial position of the stabilization point shifts radially inwards with increasing hydrogen content. This is quantified in table 5.1 which lists the mean values and standard deviations of the lift-off height and stabilization point. It appears that the flame fluctuates less with increasing hydrogen content of the fuel, as the standard deviation of the lift-off height, the axial and radial stabilization point location reduce with increasing hydrogen content. This indicates the stabilizing effect hydrogen has on the investigated flames.

5.1.2. Timescale of Axial Stabilization Point Fluctuations

As listed in table 5.1, the standard deviation of the axial stabilization point location of the investigated flames decrease with increasing hydrogen content in the fuel. The left-hand-side of figure 5.3 shows time series of the axial stabilization point location of the four investigated flames. It appears that the frequency of these fluctuations increase with increased hydrogen content. It is thought this is due to the higher reactivity of the fuel-oxidizer mixture and increased burning velocities with increasing hydrogen in the fuel.

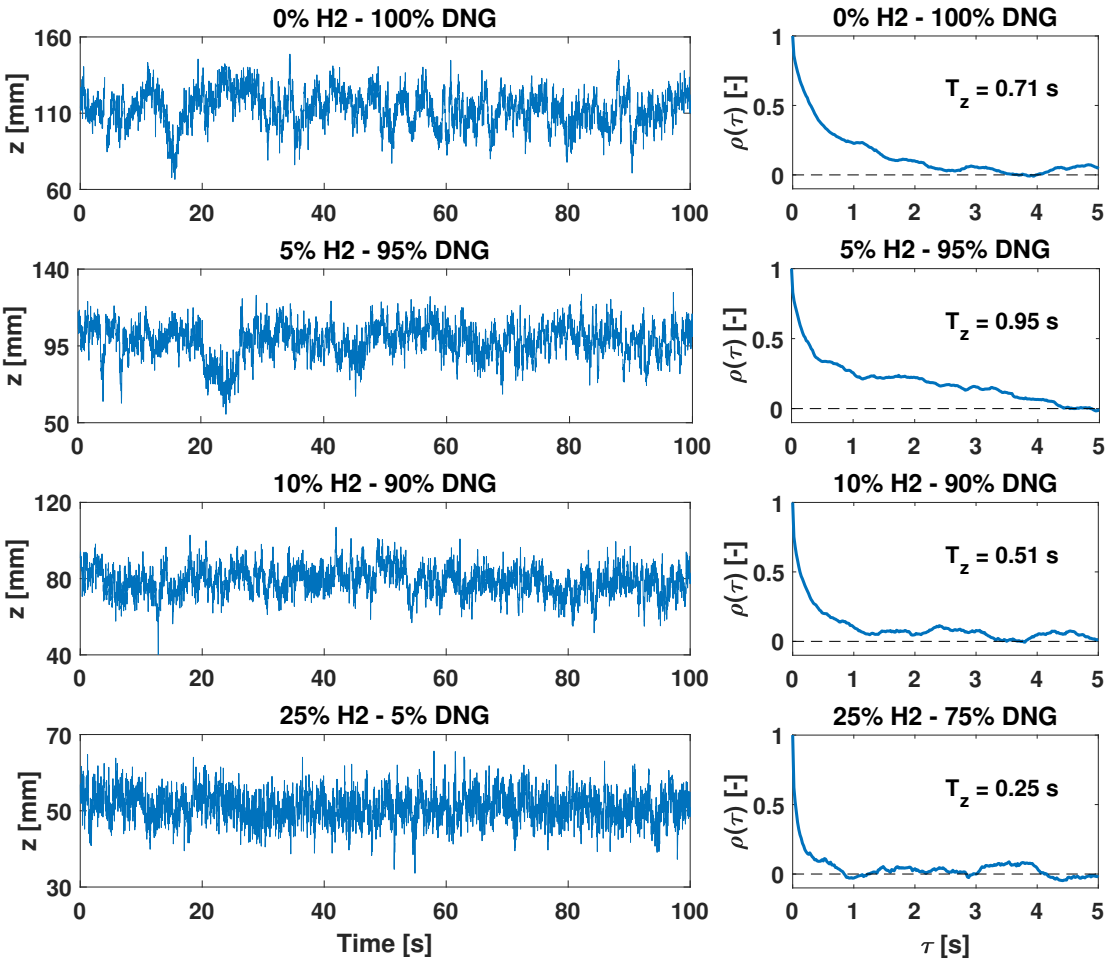

Figure 5.3: Left) Time series of the axial stabilization point location. Right) Auto-correlation functions of the axial stabilization point location.

To get insight in the integral timescale of the axial fluctuations of the investigated flames, the auto-correlation function was computed. The auto-correlation function $\rho(\tau)$ is calculated through

$$\rho(\tau) = \frac{\overline{z'(t)z'(t+\tau)}}{\overline{z'^2}}, \tag{5.2}$$

where τ is the time lag and $z'(t)$ is the fluctuation of the axial stabilization point at time t, defined as $z'(t) = z(t) - \overline{z}$, where $\overline{z}$ is the mean axial stabilization point location. From this, the integral timescale T can be derived from $\rho(\tau)$ as in

$$T_z = \int_0^\infty \rho(\tau) d\tau. \tag{5.3}$$

The right-hand-side of figure 5.3 shows the auto-correlation function of the axial stabilization point location of the investigated flames. It can be seen that the integral timescale of the axial fluctuations reduces with increasing hydrogen content in the fuel. The integral time-scale of the DNG flame is approximately three times larger than the time-scale of the 25% H_2 flame.

Information on the integral time scale T_z is also useful to determine the necessary measurement time T to reach converged statistics of the investigated flames. As for the flame with the largest integral time scale, the DNG flame, the integral time-scale of the axial fluctuations is approximately 0.7 second. So, the measurement time of 100 seconds at a sampling rate of 50 Hz is sufficient. It is also expected that the high-speed measurements will capture the statistics of the investigated flames entirely, as a 2 seconds measurement time is attained.

5.1.3. Transient Flame Behaviour

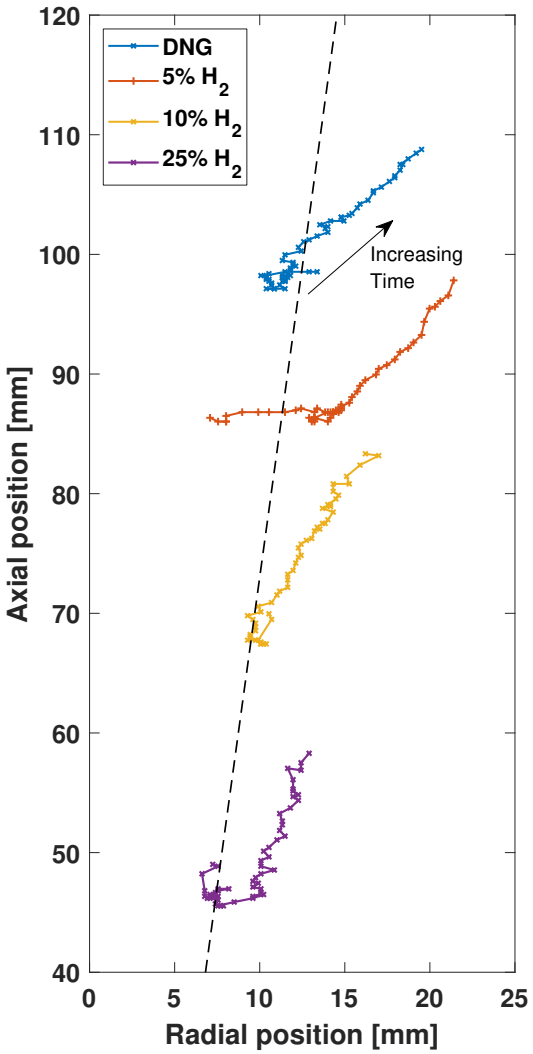

Figure 5.4: Typical trajectories of the stabilization point of the DNG and hydrogen flame cases. The dashed line represents the jet-half-width line of a theoretical turbulent jet as described by equation 5.1.

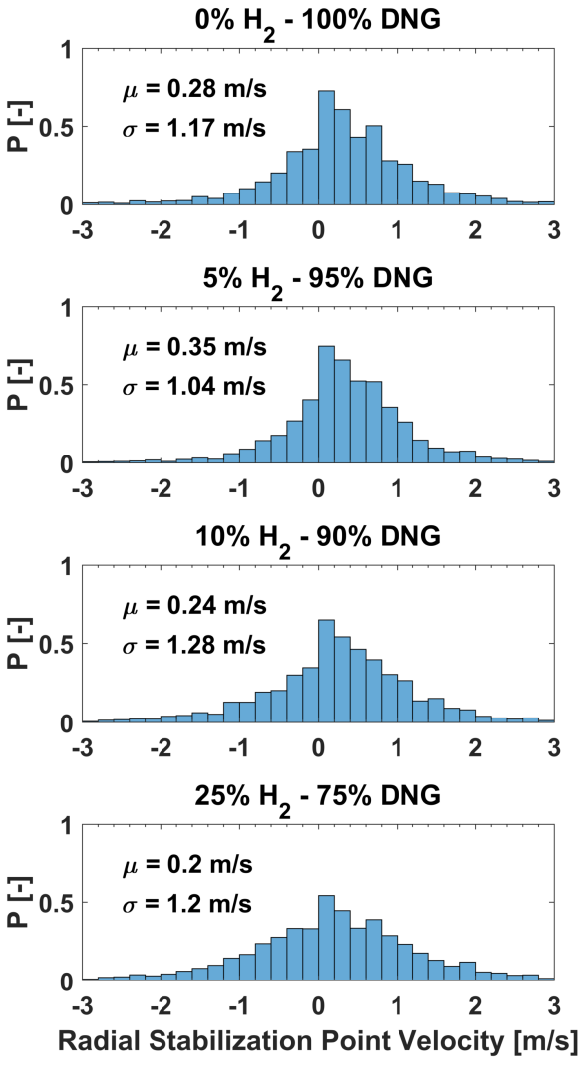

Figure 5.5: PDFs of the stabilization point velocity calculated from the stabilization point movement in x- for the DNG and hydrogen flame cases. Annotated are the mean and standard deviation of the radial stabilization point velocity.

High-speed PIV measurements at 2.5 kHz are performed to obtain insight in the effects of hydrogen on the transient behaviour of the stabilization point. The DNG and hydrogen flames are examined. For each flame, 5000 images are captured which yielded 2573, 3182, 3012 and 4164 stabilization points for the flame cases, respectively. Using the image processing procedures described in section 4.3, these stabilization points were grouped in 130, 137, 155 and 161 trajectories, respectively. Figure 5.4 shows typical trajectories of the stabilization point for the DNG and hydrogen flame cases, together with the jet-half-width (dashed line). The stabilization points move from the high-velocity side of the jet-half-width line downstream towards the low-speed region. The stabilization point trajectories appear to better align with the jet spreading line, with increasing hydrogen concentration.

In assessing the transient behaviour of the flames, it has been noticed that the motion of the stabilization point can be roughly divided in the more or less gradual displacement along the trajectory followed by sudden jumps towards the beginning of a new trajectory at an upstream and radially inward location. It is proposed this cycle describes the typical movement of the stabilization point location.

The extend at which the typical cycle dictates the motion of the stabilization point is found to be dependent on the hydrogen content. Figure 5.5 shows the PDFs and mean of the radial stabilization point velocity of the DNG and hydrogen flames. The stabilization point displacement caused by sudden jumps is excluded. The more the mean radial stabilization point velocity deviates from zero, the more sudden jumps take place displacing the stabilization point towards an upstream and radially inward location. This as a zero mean radial stabilization point velocity is expected for a statistically stationary flame. It is observed that the mean radial stabilization point velocity decreases with hydrogen. This indicates that with increasing hydrogen in the fuel, fewer stabilization point displacements can be accounted to sudden jumps. Hence, the stabilization point motion is altered with increasing hydrogen content as hydrogen is expected to promote the formation and ignition of flammable fuel-oxidizer mixture upstream of the flame front due to its high flammability and mixing capability.

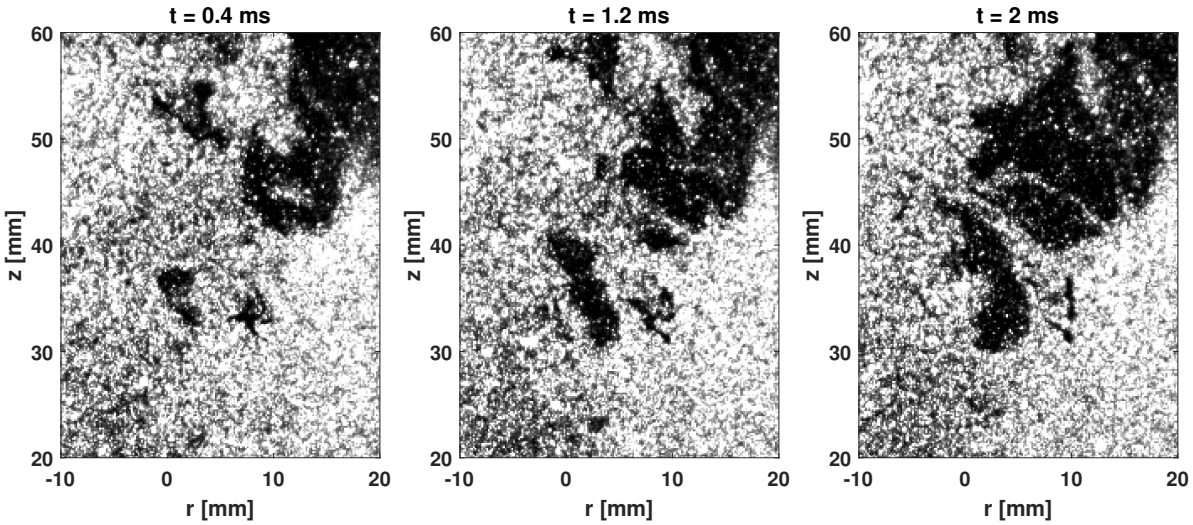

Figure 5.6: Three 10% H_2 high-speed PIV snapshots of the region around the right-hand-side stabilization point with a Δt = 0.8 ms time difference. The dense white areas represent the unburned gas region and the dense black areas the burned gas region. The sequence is exemplary for the appearance of a flame island that merge with the existing flame base.

The jump phenomena are caused by the appearance of upstream "flame islands" which merge with the flame edge. The appearance of these flame islands is likely to be caused by out-of-plane motion of the flame. Figure 5.6 shows an sequence of raw PIV images of a 10% hydrogen flame

that illustrate a jump in stabilization point location. From the left to right image, the flame island appears, grows and merges with the existing flame region. This causes the stabilization point to jump to the new upstream flame edge. Gordon *et al.* [31] conclude that approximately half of the upstream movement of the stabilization point is attributed to appearing flame islands. They also find a strong correlation between appearance of flame islands and an increase of in out-of-plane gas velocity. This points out that the jump phenomena is largely caused by out-of-plane flame motion.

5.2. Effect of Hydrogen on the Burning Velocity

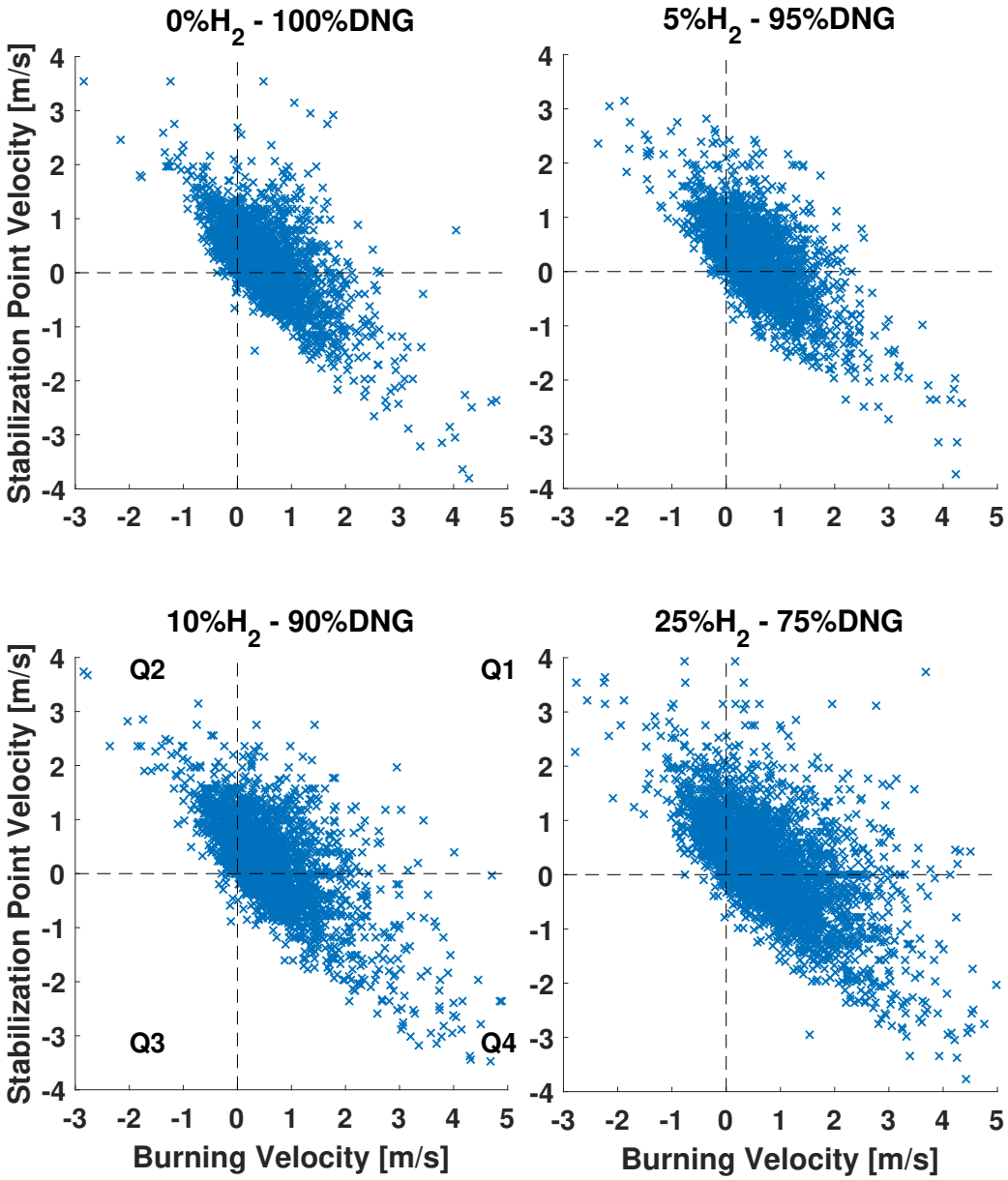

Figure 5.7: Scatter plots of the stabilization point velocity versus the burning velocity for the DNG and hydrogen flame cases. The dashed lines mark the boundaries between the four quadrants indicated by Q1, Q2, Q3 and Q4.

Flame speeds are calculated from the stabilization point trajectories and the gas velocity at a location just upstream of the stabilization point, as described in Chapter 4. Figure 5.7 shows scatter plots of the burning velocity of the DNG and hydrogen flames versus the corresponding axial sta-

bilization point velocity. The points in quadrant one and four represent downstream and upstream stabilization point movement, respectively. The points in quadrant two and three represent unfeasible flame behaviour because it is physically unrealistic to attain negative burning velocities. In general, these plots indicate a negative correlation of the stabilization point velocity with the burning velocity. This is understandable as, on average, higher burning velocities permit the flame to move upstream hence higher negative axial stabilization point velocity.

	0%H_2 - 100% DNG	5%H_2 - 95% DNG	10%H_2 - 90% DNG	25%H_2 - 75% DNG
Total [n]	2573	3182	3012	4164
Upstream [n]	846	950	995	2069
Downstream [n]	1651	2151	1923	1606
Stationary [n]	76	81	94	489

Table 5.2: Occurrences of upstream, downstream and stationary stabilization point motion per flame case.

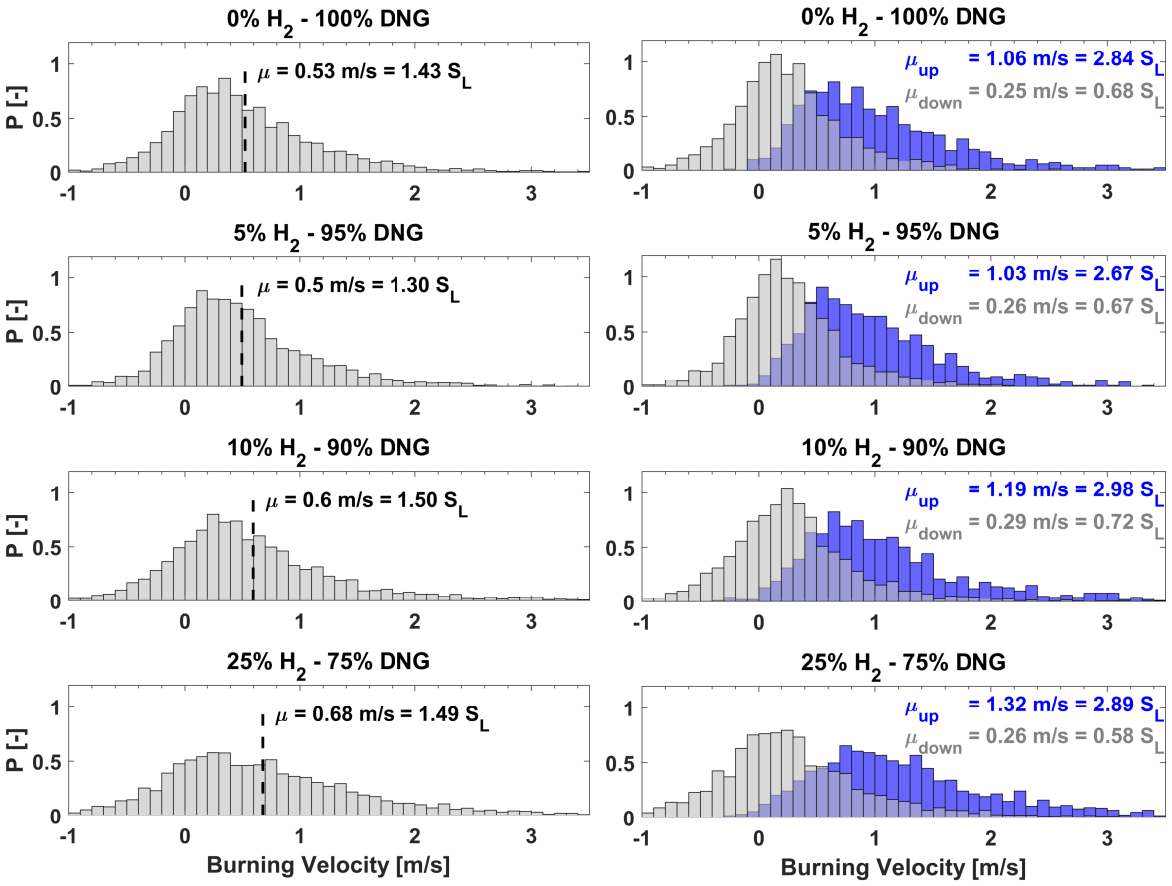

Figure 5.8: Left) PDFs of the burning velocity for the DNG and hydrogen flames. Annotated are the mean burning velocities in m/s and in terms of S_L. Right) PDFs of burning velocity conditioned on the upstream motion of the stabilization point (blue) and downstream motion of the stabilization point (gray) for the DNG and hydrogen flame cases. Annotated are the mean burning velocities in m/s and in terms of S_L.

Flame case		S_L	Burning Velocity		Upstream Motion		Downstream Motion	
		[m/s]	[m/s]	[S_L]	[m/s]	[S_L]	[m/s]	[S_L]
0% H_2	100% DNG	0.371	0.53	1.43	1.05	2.84	0.25	0.68
5% H_2	95% DNG	0.385	0.5	1.30	1.03	2.67	0.26	0.67
10% H_2	90% DNG	0.400	0.6	1.50	1.19	2.98	0.29	0.72
25% H_2	75% DNG	0.457	0.68	1.49	1.32	2.89	0.27	0.58

Table 5.3: Laminar flame speeds S_L for the DNG and hydrogen flame cases, plus the mean values of the PDFs in figure 5.8, both in m/s and in terms of S_L.

Table 5.2 displays the occurrences of upstream, downstream or stationary stabilization point movement for the DNG and hydrogen flame cases. In general, downstream stabilization point motion occurs most often, followed by upstream stabilization point motion and stationary stabilization point motion. The left of figure 5.8 shows PDFs of the burning velocity for the DNG and hydrogen flames. Table 5.3 lists the laminar flame speeds as extracted from CHEM1D [41] for the DNG and hydrogen flame cases. The table also summarizes the mean values of the PDFs of figure 5.8, both in m/s and in terms of S_L. It indicates that with increasing hydrogen in the fuel, the mean burning velocity in m/s increases. As result of the hydrogen increase in the fuel, the laminar flame speed also increases in such a way that the burning velocity in terms of S_L remains more or less constant with values between 1.3 S_L and 1.5 S_L.

The right of figure 5.8 shows the PDFs of the burning velocity conditioned on the upstream and downstream motion of the stabilization point motion for the DNG and hydrogen flame cases. It appears that the burning velocity is significantly higher in case of upstream stabilization point motion than during downstream motion. Referring to table 5.3, for upstream stabilization point movement the burning velocity in terms of S_L is around 2.7 S_L to 3.0 S_L and 0.6 S_L to 0.7 S_L for downstream movement. The large difference in burning velocity for upstream and downstream stabilization point motion is expected as the high burning velocity enables the flame to move upstream until the burning velocity equals the gas velocity. In case of downstream stabilization point motion, the burning velocity is lower than the gas velocity and moves downstream resulting in much lower burning velocities. The difference in burning velocities conditioned on the stabilization point motion is previously observed by Gordon *et al.* [31] for a propane/argon mixture at $Re = 10^4$. The current investigation shows that the fraction of hydrogen in the fuel is not impacting the difference in the burning velocity in terms of S_L when conditioned on the direction of the stabilization point motion.

5.2.1. Reproducability of the Burning Velocity Measurements

A repetition of the high-speed PIV measurement of the DNG flame is done to assess the reproducability of the derived burning velocities. The integral time-scale of a flame is indicative for the minimum measurement time required to reach converged statistics. It was decided to repeat the high-speed measurement in the DNG flame, because it has the largest integral time scale out of the investigated DNG and hydrogen flames as reported in section 5.1.2.

The repetition measurement yields 2816 useful samples out of the 5000 captured images, whereas the original set contains 2573 useful samples. Figure 5.9 shows the burning velocity PDFs as derived from the original and repetition measurement of the DNG flame. The PDFs show large resemblance and the mean burning velocity values are approximately the same. The standard deviation differs significantly due to infrequent outlying burning velocity values. Nonetheless, the assessment indicates that repeated measurements yield similar burning velocity results plus that the statistics converge in the used measurement time.

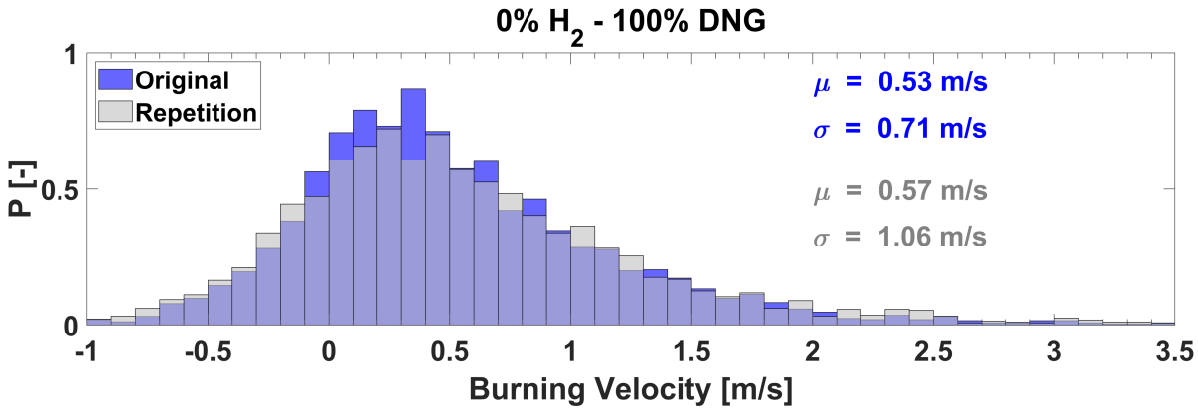

Figure 5.9: PDFs of the burning velocity for the DNG flame derived from the original (blue) and repetition (grey) high-speed measurement. Annotated are the mean and standard deviation of the original and repetition burning velocity.

5.2.2. Effect of Spatial Resolution on Burning Velocity

A zoomed-in high-speed PIV measurement of the 10% hydrogen flame with increased spatial resolution is done to assess the effect of the spatial resolution on the derived burning velocities. The 10% hydrogen flame is selected for the repetition measurement, as with this flame the largest increase in spatial resolution can be achieved. Resulting spatial resolution of the PIV measurement is 16 pixel/mm, 2.5 times larger than in the original measurement. 5000 samples are taken in the zoomed-in measurement run, from which 2019 were useful compared to 3012 in the original measurement. Clarification for this difference could be an imperfect seeding profile, resulting in a more difficult stabilization point extraction.

Figure 5.10 shows the PDFs of the burning velocity for the original and zoomed-in measurements. Both PDFs show large resemblance and the mean and standard deviation of the burning velocities are approximately equal. The measurements with the original resolution are therefore considered as accurate spatially resolved.

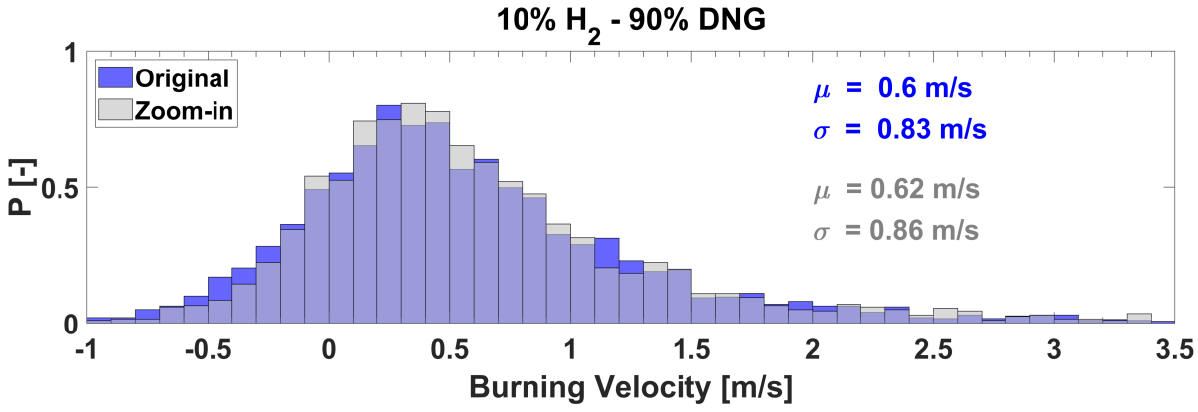

Figure 5.10: PDFs of the burning velocity derived from the original (blue) and zoomed-in (grey) high-speed measurement for the 10% hydrogen flame. Annotated are the respective mean and standard deviation of the burning velocities.

5.2.3. Reflection on Burning Velocity Results

The negative burning velocities that were reported in figures 5.7 and 5.8 are physically unrealistic and must be an artifact of the procedure used to derive the burning velocities. Most probably this results from out-of-plane flame motion. Three-dimensional flame motion causes an out-of-plane motion through the fixed PIV plane distorting the obtained stabilization point velocity and so the obtained burning velocity. To illustrate this, we assume for simplicity that the flame has a fixed

three-dimensional funnel-shaped structure that moves through the PIV plane in the out-of-plane direction. The lowest point of resulting cross-section of the flame and the PIV plane appears to move erroneously upstream or downstream as result of this out-of-planar motion. As the stabilization point velocity and burning velocity derives from the stabilization point motion in this plane, both quantities contain a continuous error due to the out-of-plane motion in combination with a planar measurement approach. Literature confirms this, as Upatnieks *et al.* [30] applied the same method to obtain burning velocities in which they also report negative burning velocities. They point towards out-of-plane flame motion as a source of error in the obtained burning velocities. Likewise, Gordon *et al.* [31] use the same burning velocity calculation procedure as in this study, whereas they exclude stabilization point locations influenced by the out-of-plane motion. This is done by measuring the out-of-plane gas velocity upstream of the stabilization point corresponding to the derived burning velocity by using a combined stereo-PIV and OH-PLIF measurement system. Following this procedure, Gordon *et al.* [31] only reports upstream directed (positive) burning velocities.

Another hypothesis is that the burning velocity is affected by a possible discrepancy between the assumed and the actual stabilization point location. Joedicke *et al.* [33] conclude that the flame stabilizes in the mixing layer of the jet at locations where the fuel-oxidizer mixture is 1.1 times the stoichiometric mixture fraction. Su *et al.* [36] suggest the stabilization point is located jet-inwards and slightly downstream of the most upstream point of the flame region. The latter is assumed to be the stabilization point in this investigation. This alternative location of the stabilization point is in a region with a higher gas velocity and hence higher stabilization point velocities.

5.3. Effect of Hydrogen on Conditions at the Stabilization Point

5.3.1. Local Flow Field Statistics

The statistics of the flow field at a rectangular region with size 1.25 mm x 1.25 mm located 1.25 mm upstream of the stabilization point is derived from the high-speed PIV measurements at 2.5 kHz for the DNG and hydrogen flame cases. The axial gas velocity is extracted from the PIV vector fields of the assessed flame cases. The vorticity in the *zr*-plane is calculated from equation 5.4 and the divergence from equation 5.5, assuming incompressible flow. In addition, for all these quantities the mean statistics fields conditioned around the stabilization point location are derived. The statistics fields are determined by summing the statistics derived from a 8 by 8 cluster of PIV interrogation areas around the stabilization point for each individual velocity field. This is averaged, yielding a 10 mm x 10 mm statistics field, as the size a PIV interrogation area is 1.25 mm by 1.25 mm. For the readers orientation, the right-hand-side stabilization point of the investigated flame is subject of attention, hence the fuel jet is located on the left of the field.

$$\omega_z = \frac{\partial u_z}{\partial r} - \frac{\partial u_r}{\partial z} \tag{5.4}$$

$$\nabla \cdot \vec{u} = \frac{\partial u_r}{\partial r} + \frac{\partial u_z}{\partial z} = 0 \tag{5.5}$$

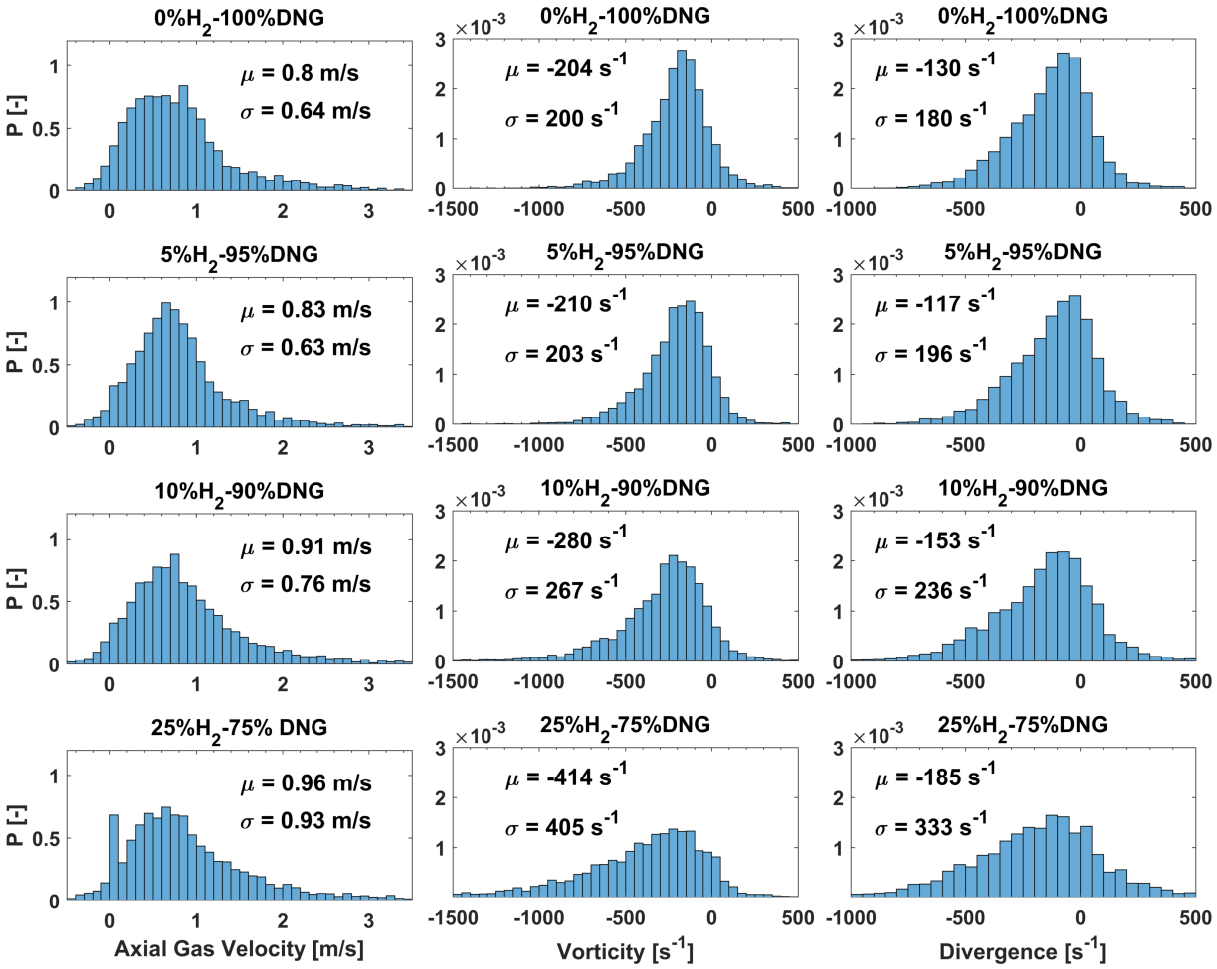

Figure 5.11: Statistics of the flow field 1.25 mm upstream of the stabilization point for the DNG and hydrogen flame cases. Left) PDFs of the axial gas velocity with annotated mean value and standard deviation. Middle) PDFs of the vorticity with mean value and standard deviation. Right) PDFs of the divergence with mean value and standard deviation.

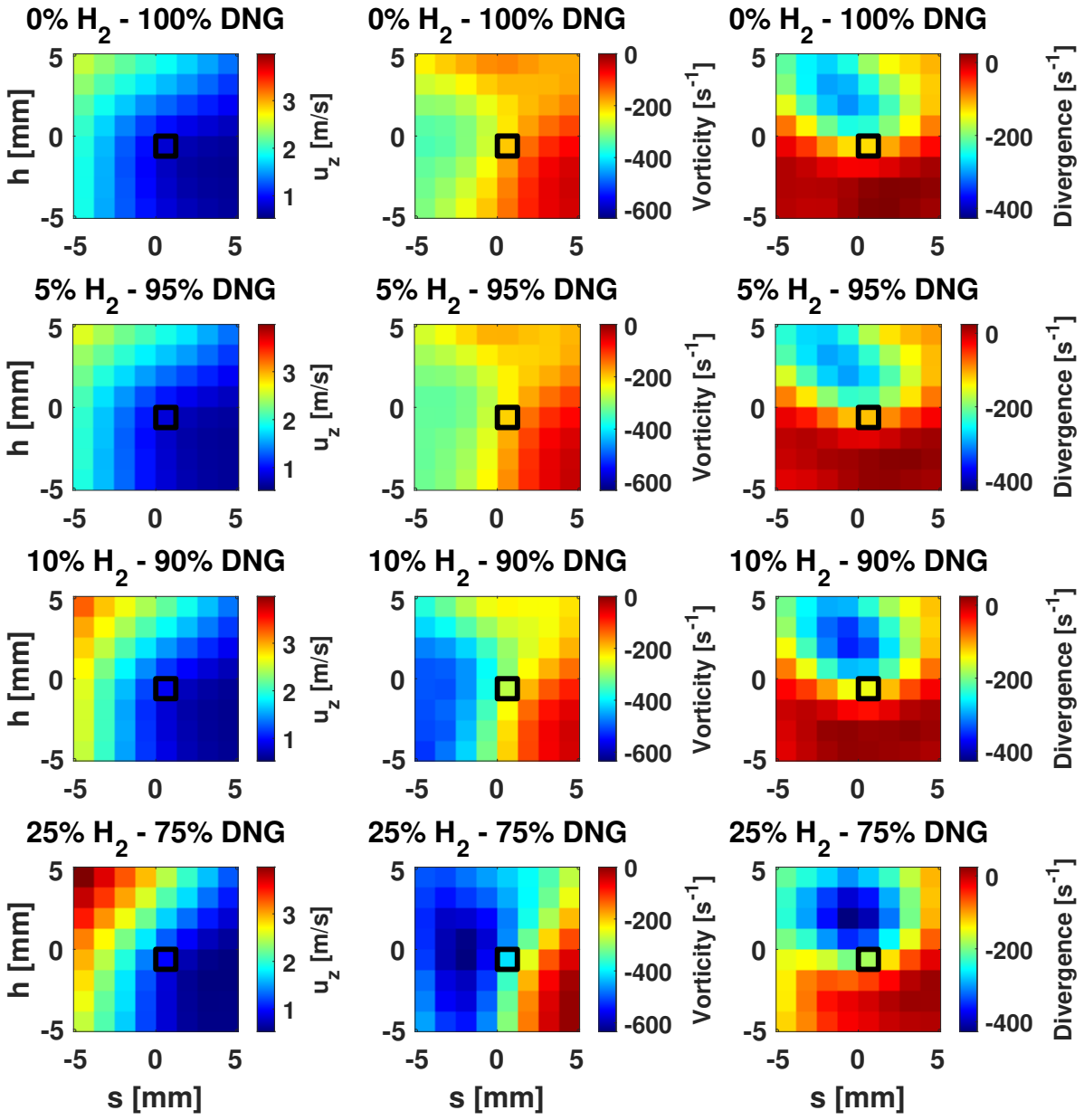

Figure 5.12: Mean flow statistics fields conditioned around the right-hand-side stabilization point of the DNG and hydrogen flame cases. h and s represent the axial and radial coordinate (in mm), respectively, relative to the stabilization point location. Left) Mean axial gas velocity. Middle) Mean vorticity. Right) Mean divergence.

Figure 5.11 shows the PDFs of the instantaneous statistics of the axial gas velocity, vorticity and divergence as determined from a 1.25 mm x 1.25 mm (8 x 8 pixels) box located 1.25 mm upstream of the stabilization point for the DNG and hydrogen flame cases. The PDFs at the left of figure 5.11 show an increase in axial gas velocity with higher hydrogen content in the fuel. The mean of the axial gas velocity increases with 20% from the DNG flame to the 25% hydrogen flame, whereas the laminar flame speed S_L of these flames increase with 23%, see table 3.3. The PDFs in the middle column of figure 5.11 show that the vorticity increases with increasing hydrogen content in the fuel. This increase is significant as the mean vorticity of the 25% hydrogen flame is twice as high compared to the pure DNG flame. It indicates that hydrogen enables the flame to stabilize in regions with significantly higher vorticity. The PDF at the right of figure 5.11 show negative divergence, becoming more negative with increasing hydrogen content in the fuel. Gordon *et al.* [31] also observed nega-

tive divergence upstream of the stabilization point for lifted propane/argon flames, in such that the influence of out-of-plane flame motion is excluded. Current finding does not align with the stability proposition of Upatnieks *et al.* [30] that states the heat released by the flame induces divergence upstream of the stabilization point. This would lead to a low velocity and low turbulence region directly upstream of the stabilization point.

Figure 5.12 shows the mean statistics field of the axial gas velocity, vorticity and divergence conditioned around the stabilization point for the DNG and hydrogen flame cases. The black rectangle indicates the interrogation area from which the data presented in figure 5.11 is extracted. The left fields of figure 5.12 shows that the mean axial gas velocity around the stabilization point increases with higher hydrogen content in the fuel. It appears that the stabilization point is located in the flow region characterized by the transition from high to low axial gas velocity. The fields in the middle of figure 5.12 show a high mean vorticity at the fuel jet side of the stabilization point, increasing with augmented hydrogen content of the flame. It seems that the stabilization point is located in the shear layer of the fuel jet and coflow in which the transition takes place from high vorticity jet-inwards to lower vorticity jet-outwards. The right fields of figure 5.12 show negative divergence downstream of the stabilization point, increasing with hydrogen content of the fuel. Very small negative divergence values are observed upstream of the stabilization point regardless of hydrogen content of the flames. This rejects the theory of Upatnieks *et al.* [30] stating that the flame stabilizes due to a low velocity and low turbulence region just upstream of the stabilization point due to combustion heat induced divergence. Furthermore, the here presented mean statistics fields shows strong resemblance to the statistics fields obtained by Gordon *et al.* [31] for propane/argon flames.

5.3.2. Time Averaged Velocity Fields

Figure 5.13 shows time-averaged velocity fields (the right-hand-side only) of the DNG and hydrogen flame cases derived from the 2.5 kHz PIV measurements. The averaged stabilization point location is indicated by a black box. The time-averaged velocity fields are cut-off at velocities above 4 m/s and these regions are shown in dark red. This as PIV is unable to accurately capture both the high velocity jet region and the low velocity region around the stabilization point, because these velocities differ by a factor of 40.

Figure 5.13 shows from left to right, from top to bottom, the time-averaged velocity fields of the DNG flame and its repetition measurement, the 5% hydrogen flame, the 10% hydrogen flame, the increased spatial resolution measurement of the 10% hydrogen flame and the 25% hydrogen flame. The white dashed lines indicate the area zoomed in for the increased spatial resolution measurement of the 10% hydrogen flame. It shows that the time-averaged stabilization point is located in a transition region from high to low velocity, regardless of the hydrogen content of the flame. High velocities are observed spreading radially outwards directly downstream of the stabilization point. This as combustion takes place directly downstream of the stabilization point location, propelling combustion products downstream. The velocity field of the DNG repetition resembles the velocity field of the original DNG flame measurement, with only a slightly altered time-averaged stabilization point location. The same can be said about the velocity field of the measurement of the 10% hydrogen flame with higher spatial PIV resolution and the velocity field of the original 10% hydrogen flame measurement.

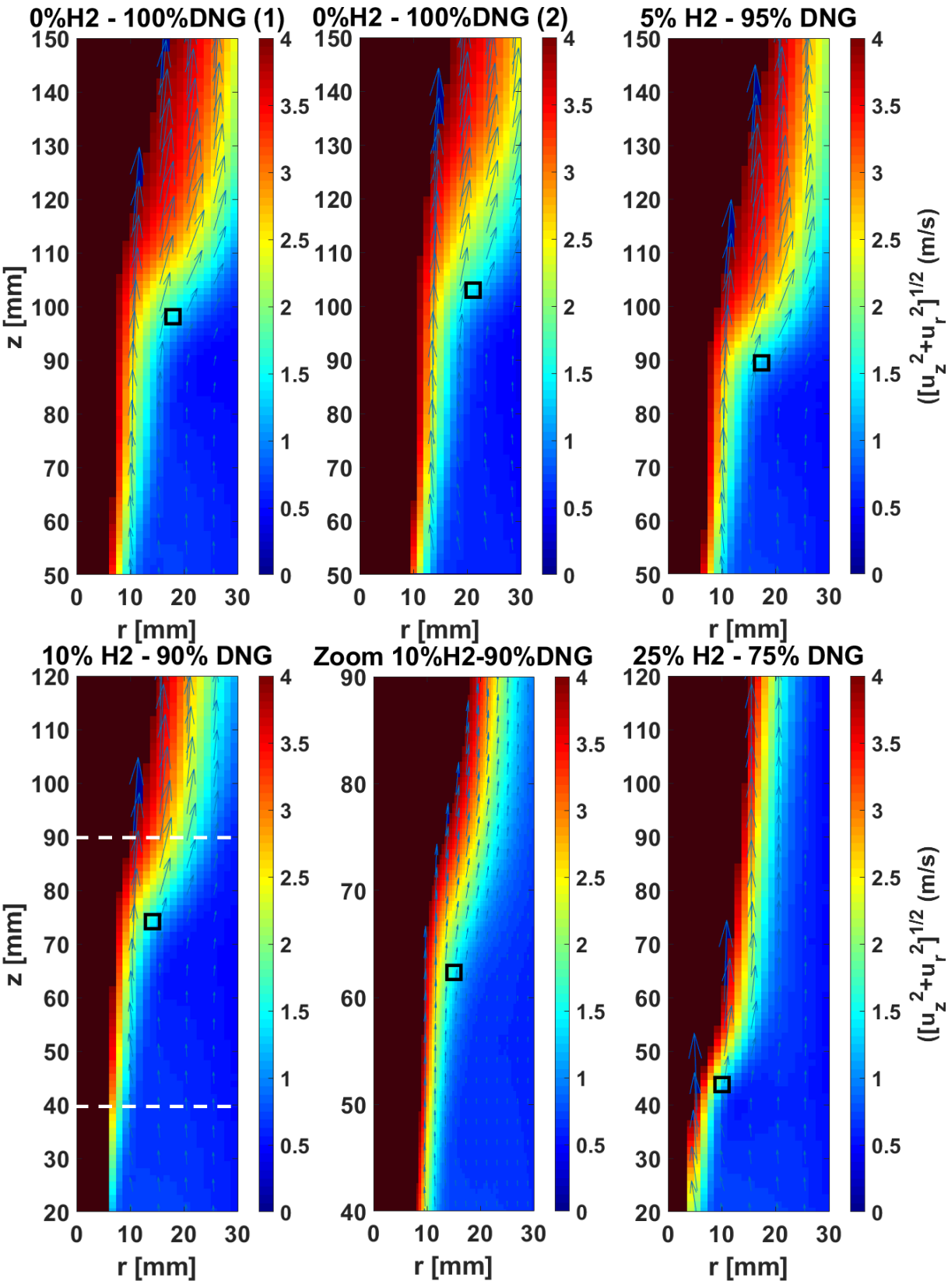

Figure 5.13: Time-averaged velocity fields of the DNG and hydrogen flame cases, plus a zoom in of the 10% hydrogen flame. The average stabilization point location is indicated by a black square. The dark red in the jet-core indicates velocities over 4 m/s. From left to right and top to bottom: Original DNG, repetition DNG, 5% hydrogen, 10% hydrogen flame with the dashed lines indicating the zoomed-in area, zoomed-in 10% hydrogen, and 25% hydrogen flame.

5.4. Effects of CO_2 on Flame Stabilization

5.4.1. Lift-off Height and Stabilization Point Location

PIV and OH* images are recorded to determine the lift-off height and stabilization point location under influence of coflow CO_2 dilution of the coflow. Two CO_2 flames are defined as listed in table 3.3 (on page 15) and these will be compared to the 25% hydrogen flame without CO_2 in the coflow.

Figure 5.14 shows the scatter plots of the stabilization point location (red) and the lift-off height (blue) for the 25% hydrogen reference flame and the CO_2 flame cases. It shows that with increasing CO_2 dilution, the flame stabilizes at more downstream and radially outward location. This is confirmed by figure 5.15 showing the PDFs of the lift-off height plus the axial and radial position of the stabilization point. The mean and standard deviation values of these PDFs are listed in table 5.4. It shows that the standard deviations of the lift-off height and the axial and radial stabilization point location increase under influence of CO_2 dilution of the coflow. The implies that the flame increasingly fluctuates with increasing CO_2 coflow-dilution.

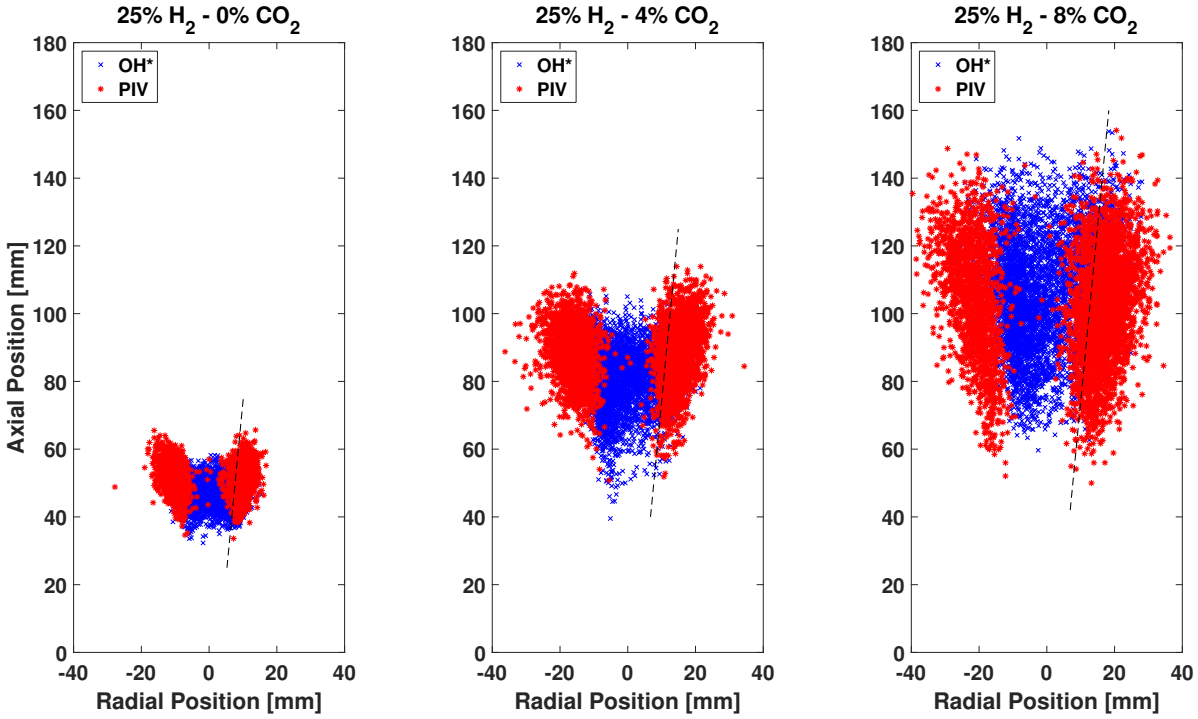

Figure 5.14: Scatter plots of lift-off heights extracted from OH* images (blue) and stabilization point locations extracted from PIV images (red) of the the 25% hydrogen flame without CO_2 dilution and the CO_2 flame cases. The dashed line represents the jet-half-width.

Flame Case		OH* Axial		PIV Axial		PIV Radial	
		μ [mm]	σ [mm]	μ [mm]	σ [mm]	μ [mm]	σ [mm]
25% H_2	0% CO_2	47.1	3.7	60	4.1	9.8	1.8
25% H_2	4% CO_2	81.4	8.6	88.3	8.6	15.2	3.6
25% H_2	8% CO_2	106.5	16.3	102.9	16.4	16.9	5.2

Table 5.4: Mean and standard deviation of the lift-off height (from OH*) and the axial and radial stabilization point location (from PIV) of the 25% hydrogen reference flame and the CO_2 flame cases.

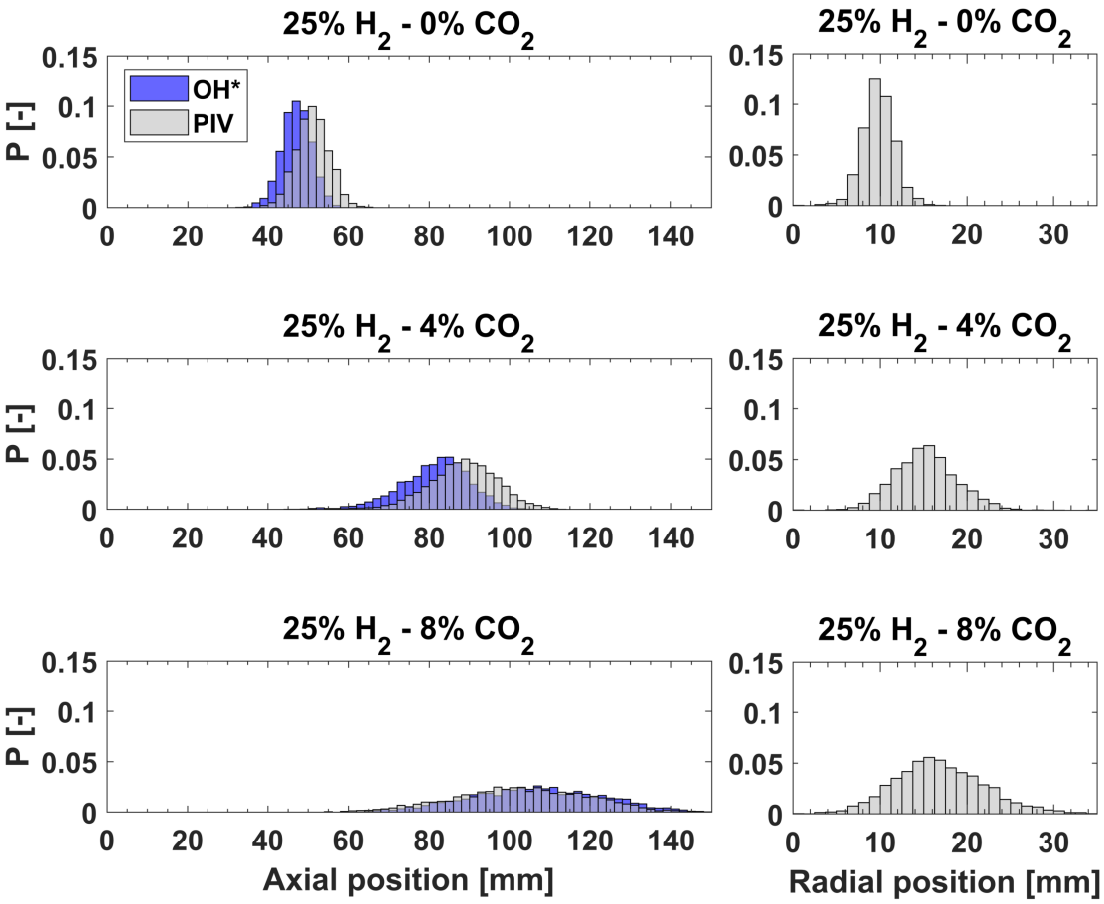

Figure 5.15: Left) PDFs of the lift-off height (blue) and PDFs of the the axial stabilization point location (grey) for the 25% hydrogen reference flame and the CO_2 flame cases. Right) PDFs of radial stabilization point location (grey) for the 25% hydrogen reference flame and the CO_2 flame cases.

It is evident that CO_2 dilution of the coflow has a destabilizing effect. It is thought the destabilizing effect of CO_2 can be attributed to the reduction of the laminar flame speed as a result of CO_2 coflow-dilution. Table 3.3 lists the from CHEM1D [41] extracted laminar flame speeds of the 25% hydrogen reference flame and the two CO_2 flame cases. The laminar flame speeds drop from 0.46 m/s for the 25% hydrogen flame without CO_2, to 0.36 m/s and 0.27 m/s for the 25% H_2 flames with 4% and 8% CO_2 in the coflow, respectively. This is thought to happen as the reactivity of the fuel-oxidizer mixture lowers due to dilution of the oxidizer flow. Referring to the flame stabilization model in which flame stability is guaranteed if the local burning velocity matches the local gas velocity, the downstream shift of a flame under influence of CO_2 coflow-dilution stabilizes again in a flow region with lower flow speeds. This perception is shared by Min and Baillot [27] in studying a lifted methane jet diffusion flame with CO_2-coflow dilution. Nonetheless, Marin and Baillot [28] suggest that the increased lift-off height is solely caused by the burning velocity reduction as result of CO_2 coflow-dilution in a lifted methane jet diffusion flame. Opposed to what is observed in current investigation, Marin and Baillot [28] do not observe an increase in radial stabilization point position with augmented CO_2 coflow dilution.

5.4.2. Burning Velocity

Burning velocities for the CO_2 flames are calculated from the high-speed PIV images, using the same procedure as for the DNG and hydrogen flame cases. The high-speed PIV measurements were conducted at 2.5 kHz and 5000 images were recorded for each flame case. The case with the 8% CO_2 was done twice to assess the reproducability of the measurements. From the 5000 recorded PIV images, 3449, 2771 and 2581 samples are used in determining the burning velocity of the flame cases 4%CO_2, 8%CO_2 and 8%CO_2-repetition, respectively.

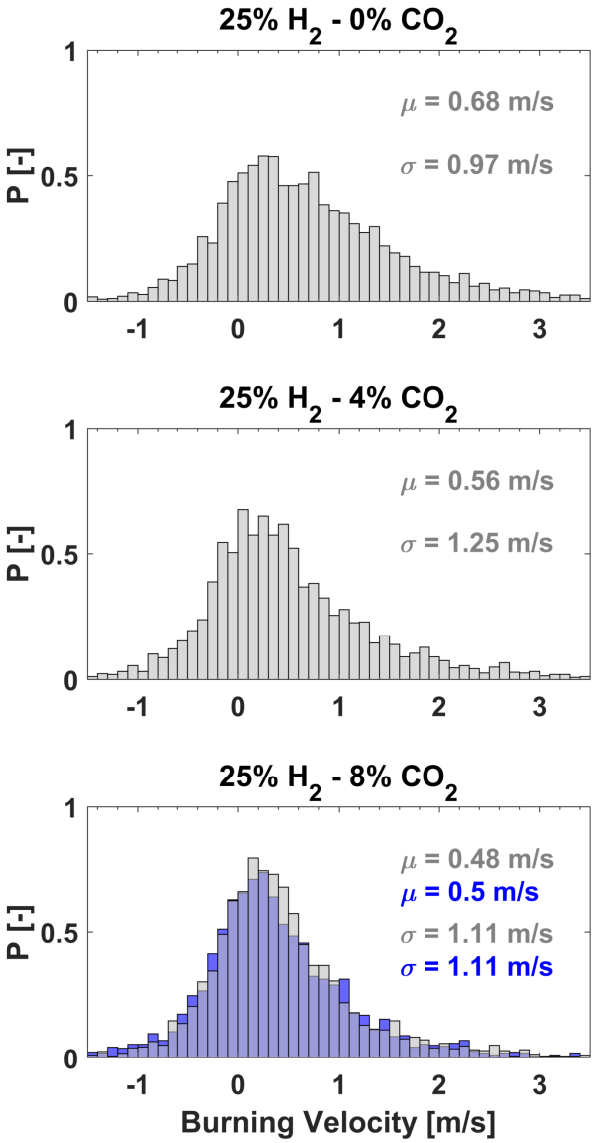

Figure 5.16: The PDFs of the burning velocity of the 25% hydrogen flame without CO_2 dilution and the CO_2 flames, with annotated mean and standard deviation value. The PDF of the 8%CO_2 repetition measurement is shown in blue.

Figure 5.16 shows the PDFs of the burning velocity of the 25% hydrogen flame without CO_2 dilution and the two CO_2 flames. The PDF of the 8%CO_2 repetition measurement is shown in blue. The effect of CO_2-coflow dilution on the burning velocity is investigated, with the presumption that CO_2 coflow-dilution reduces the burning velocity. The PDFs show that the mean value of the burning velocity decreases with increasing CO_2 concentration in the coflow. It appears that there is no clear effect of the CO_2 concentration on the spread of the burning velocity. The burning velocities derived from the original and repetition 8% CO_2 measurement results are nearly similar.

5.4.3. Flow Field Statistics

Statistics of the flow field was determined at a rectengular box with size 1.25 mm x 1.25 mm located 1.25 mm upstream of the stabilization point is derived from the high-speed PIV measurements at 2.5 kHz. As for the hydrogen flame cases in section 5.3.1, three statistical quantities are assessed for the 25% hydrogen flame without CO_2 dilution and the two CO_2 flames. Namely the axial gas velocity, vorticity and divergence. Similarly as for the DNG and hydrogen flame cases, the axial gas velocity is extracted from the PIV velocity fields of the assessed flame cases, the vorticity in the *zr*-plane is calculated from equation 5.4 and the divergence from equation 5.5 assuming incompressible flow. The mean statistics fields of the axial gas velocity, vorticity and divergence are constructed from the high-speed PIV measurements. The statistics fields are determined by summing the statistics derived from 8 x 8 PIV interrogation areas around the stabilization point for each individual velocity field. This is averaged, yielding a 10 mm x 10 mm statistics field, as the size a PIV interrogation area is 1.25 by 1.25 mm. The right-hand-side stabilization point of the investigated flames is centre of attention.

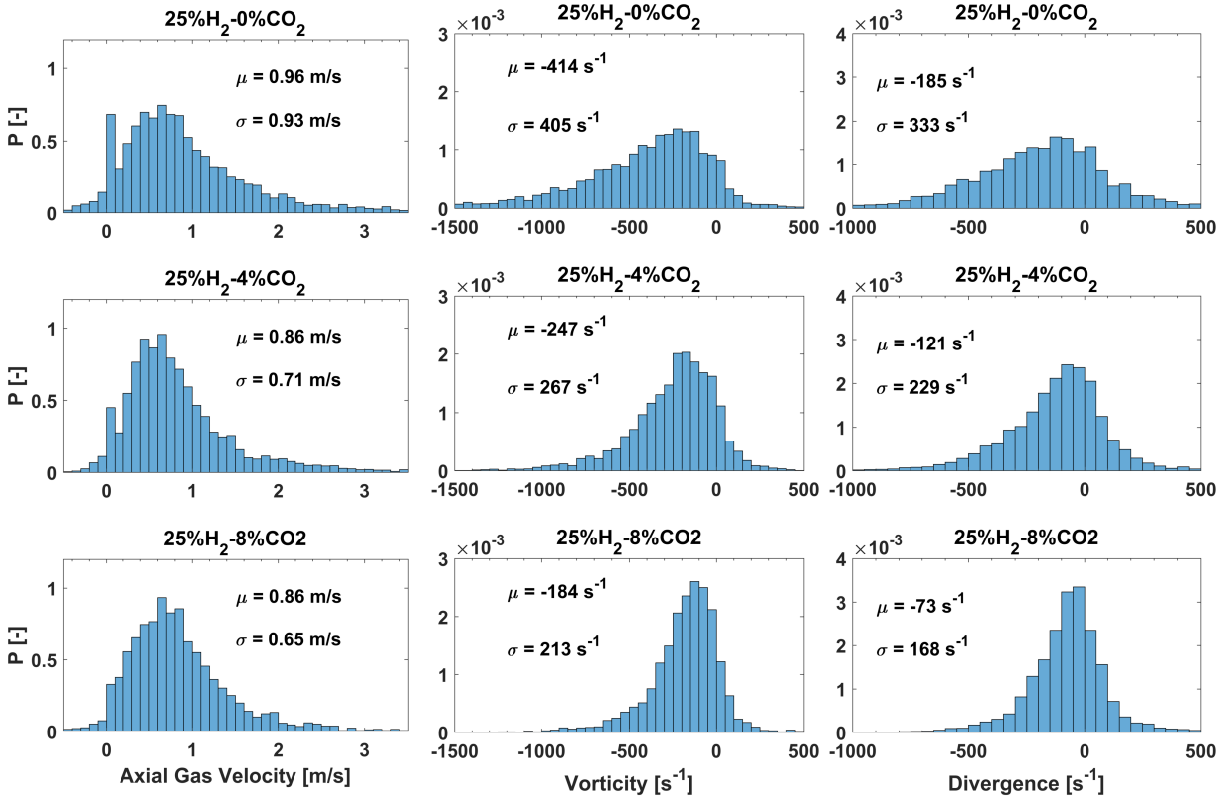

Figure 5.17: Statistics of the flow field 1.25 mm upstream of the stabilization point of the 25% hydrogen flame without CO_2 dilution and the CO_2 flames. Left) PDFs of the axial gas velocity with annotated mean value and standard deviation. Middle) PDFs of the vorticity with mean value and standard deviation. Right) PDFs of the divergence with mean value and standard deviation.

Figure 5.17 shows the PDFs of the axial gas velocity (left column), vorticity (centre) and divergence (right) for the 25% hydrogen flame without CO_2 dilution and the CO_2 flames. The PDFs on the left of figure 5.17 indicate a decrease in axial gas velocity from the 25% hydrogen flame without hydrogen coflow dilution to the CO_2 flame cases. However, increasing the CO_2 level in the coflow from 4% to 8% has no significant influence on the axial velocity. This is in contrast to the earlier observation flame that the 8% CO_2 flame stabilizes at a more downstream position than the 4% CO_2 flame. Lower axial gas velocities are expected for the 8% CO_2 flame if adhered to the simple stabilization model of matching gas velocity and burning velocity. The PDFs in the centre of figure 5.17 show

that vorticity upstream the stabilization point reduces with increased CO_2 in the coflow, at significant rates as illustrated by the 55% drop of the mean vorticity from the 25% hydrogen flame without CO_2 dilution to the 8% hydrogen flame. Hence it reduces the ability of the flame to stabilize flow regions characterized by high vorticity. The right PDFs of figure 5.17 show that the negative divergence found upstream the stabilization point reduces with increasing CO_2 coflow-dilution. Figure 5.17 shows that the effect of CO_2 coflow-dilution on the axial gas velocity, vorticity and divergence is opposite to the effect of hydrogen in the fuel-gas.

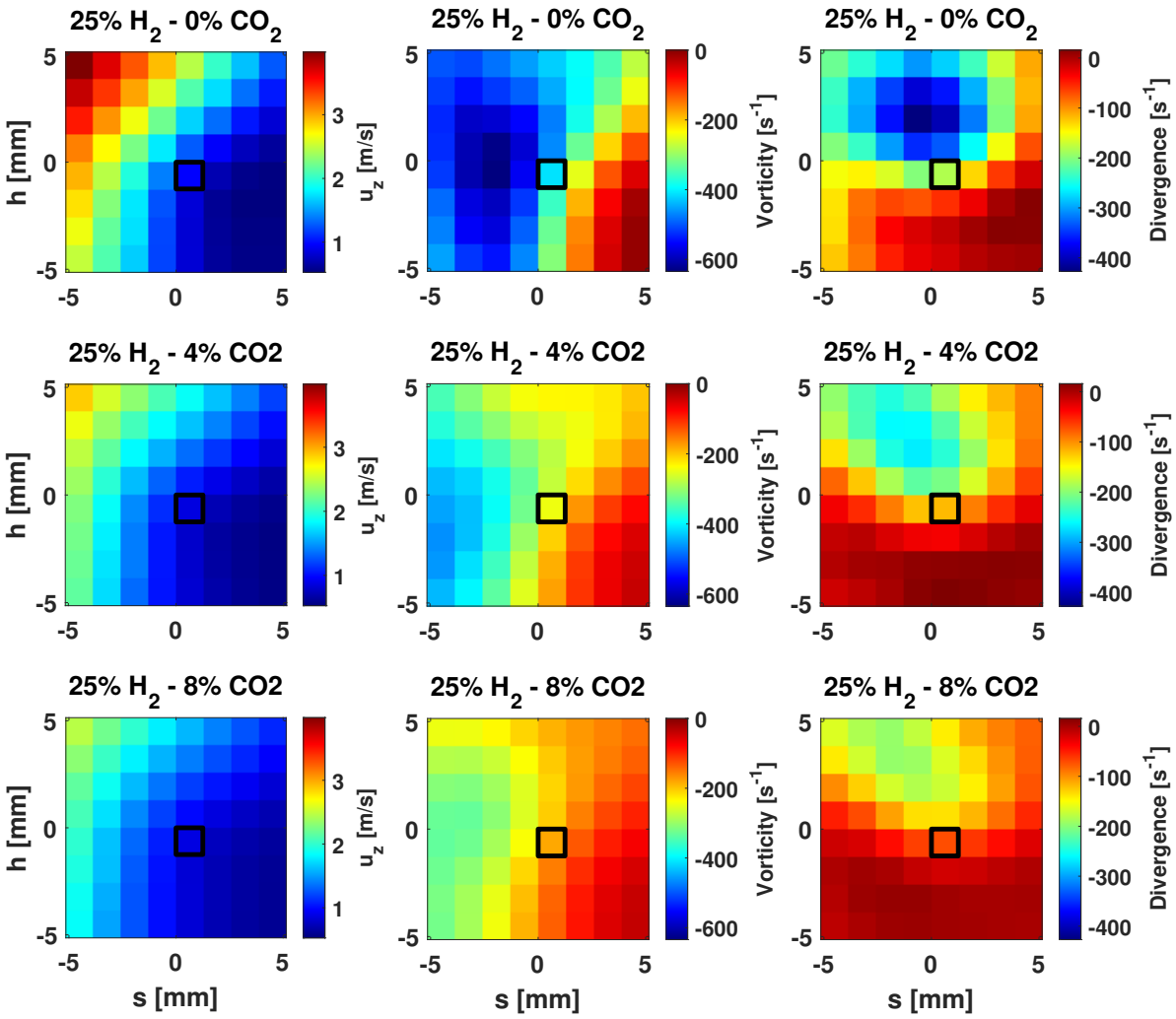

Figure 5.18: Mean flow statistics fields conditioned around the right-hand-side stabilization point of the 0% CO_2 (top), 4% CO_2 (central) and 8% CO_2 (bottom) flame cases. h and s represent the axial and radial coordinate (in mm), respectively, relative to the stabilization point location. Left) Mean axial gas velocity values. Middle) Mean vorticity values. Right) Mean divergence values.

Figure 5.18 shows the mean statistics field of the axial gas velocity, the vorticity and the divergence for the 25% hydrogen flame without CO_2 dilution and the two CO_2 flame cases. The black rectangle indicates the interrogation area from which the data presented in figure 5.17 is extracted. The left fields of figure 5.18 show that the axial gas velocity around the stabilization point reduces with increasing CO_2 coflow-dilution. The inner-jet region is clearly recognizable by the high velocities. It can be seen that with increasing CO_2 in the coflow, the mean stabilization point location is farther away from this high-velocity part of the fuel jet. The middle fields of figure 5.18 show that the vorticity reduces around the stabilization point location, especially towards the jet-inner

region. The mean location of the stabilization point appears to be at the shear layer of the coflow and the fuel-jet, characterized by the transition from high to low vorticity. The right fields of figure 5.18 show the distribution of divergence around the stabilization point. Negative divergence is observed downstream of the mean stabilization point location as this is the burned gas region, wherein the divergence becomes less negative with increasing CO_2 content in the coflow. Upstream of the stabilization point location, the divergence has very small values indicating incompressible flow.

5.4.4. Reflection on Measurement Limits

The current experimental setup is limited in determining the stabilization point from PIV measurements of flames with a high degree of CO_2 coflow-dilution and/or in combination with low hydrogen in the fuel. This since the seeding particles used in the PIV measurements are not able to visualize the unburned gas region of a flame when the flame stabilizes at a large distance from the burner. Reason is that increasing the CO_2 coflow-dilution leads to lower flame stability and a more downstream stabilization point location, whereas the more hydrogen in the fuel the more the flame stabilizes at a upstream position. As of yet, it is possible to investigate flames with a CO_2 coflow-dilution volume percentage up to 8% CO_2 in combination with 25% hydrogen in the fuel.

5.5. Effect of the Laminar Flame Speed on Flame Stabilization

As it is thought that flame stability occurs when the local gas velocity equals the burning velocity and the burning velocity is related to the laminar flame speed, it is expected that flames with a identical laminar flame speed stabilize at the same position. To investigate this, two flames are defined with 4% and 8% CO_2 in the coflow, respectively, with hydrogen fuel-fractions such that the laminar flame speed as simulated in CHEM1D [41] equals the laminar flame speed of the 25% hydrogen flame without CO_2 in the coflow. This resulted in two flames: 45% hydrogen - 4% CO_2 flame and a 60% hydrogen - 8 % CO_2 flame, referred to as the high-hydrogen flame cases. The flame properties are tabulated in table 5.5 along with those of the 25% hydrogen flame without CO_2 in the coflow. The mole fractions and the set flow rates are listed in the tables 5.6 and 5.7, respectively.

Flame	CO_2	Re_{fuel}	u_{fuel}	$\dot{m}_{fuel}$	P	S_L	Z_{st}	T_{ad}
	[%]	[-]	[m/s]	[g/s]	[kW]	[m/s]	[-]	[K]
25% H_2	0	5923	26.3	2.44	10.2	0.457	0.0665	2220
45% H_2	4	6000	34	2.43	12.5	0.454	0.059	2159
60% H_2	8	6000	42.9	2.39	13.6	0.451	0.052	2098

Table 5.5: Flame properties of the 25% hydrogen flame without CO_2 in the coflow and the two high-hydrogen flames: the fuel jet Reynolds number (Re_{fuel}), the fuel jet bulk velocity (u_{fuel}) in m/s, the fuel mass flow rate ($\dot{m}_{fuel}$) in g/s, the power output of the flame (P) in kW, the laminar flame speed (S_L) in m/s, the stoichiometric mixture fraction (Z_{st}) and the adiabatic flame temperature (T_{ad}) in K.

Figure 5.19 shows the scatter plots of the lift-off height and stabilization point location for the 25% hydrogen flame without CO_2 coflow dilution and the two high-hydrogen flames. It is seen that despite the identical laminar flame speed, the 25% hydrogen flame without CO_2 dilution stabilizes at a more downstream position than the 45% hydrogen - 4% CO_2 flame, which in turn stabilizes at a more downstream position than the 60% hydrogen - 8% CO_2 flame. Figure 5.20 shows the PDFs of the lift-off height, the axial stabilization point position and radial stabilization point location of respective flames confirming former observation. Table 5.8 lists the mean and standard deviation values. It appears that an identical laminar flame speed does not lead to the same lift-off height nor stabilization point position.

Flame	25% H_2 0% CO_2	45% H_2 4% CO_2	60% H_2 8% CO_2
	Fuel Composition x_i [-]		
CH_4	0.61	0.447	0.325
N_2	0.108	0.079	0.058
C_2H_6	0.028	0.02	0.015
H_2	0.25	0.45	0.6
Rest	0.005	0.003	0.002
	Coflow Composition x_i [-]		
O_2	0.21	0.202	0.193
N_2	0.79	0.758	0.727
CO_2	0	0.04	0.08

Table 5.6: Mole fractions of the 25% hydrogen flame without CO_2 in the coflow and the high-hydrogen flames for the fuel and coflow flows.

Flame	25% H_2 0% CO_2	45% H_2 4% CO_2	60% H_2 8% CO_2
	Fuel Flow Rate [nl/min]		
DNG	17.28	16.4	15.05
Uncertainty	0.136	0.132	0.125
H_2	5.77	13.42	22.58
Uncertainty	0.0539	0.0921	0.138
	Coflow Flow Rate [nl/min]		
Air	150	144.0	138.0
Uncertainty	1.25	1.22	1.19
CO_2	0	6	12
Uncertainty	-	0.09	0.12

Table 5.7: Set flow rates of coflow and fuel flow of the 25% hydrogen flame without CO_2 in the coflow and high-hydrogen flames with uncertainties in nl/min.

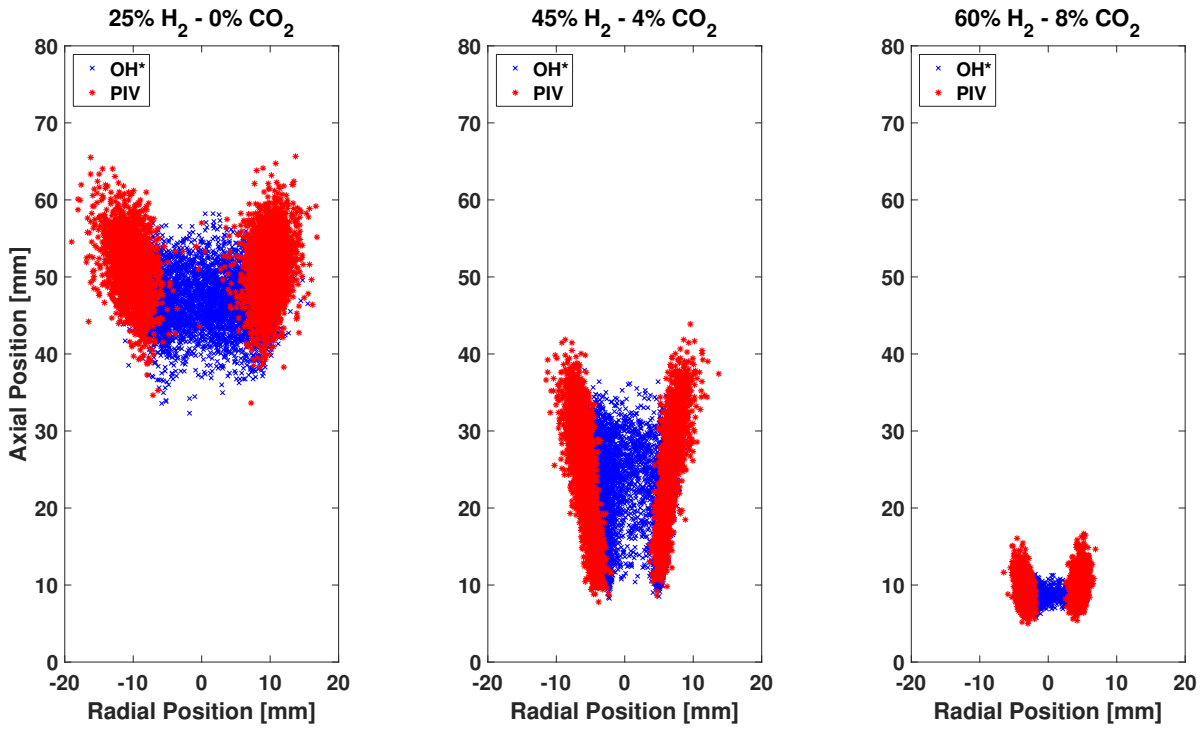

Figure 5.19: Scatter plots of lift-off heights extracted from OH* images (blue) and stabilization point locations extracted from PIV images (red) of the the 25% hydrogen flame without CO_2 dilution and the two high-hydrogen flame cases.

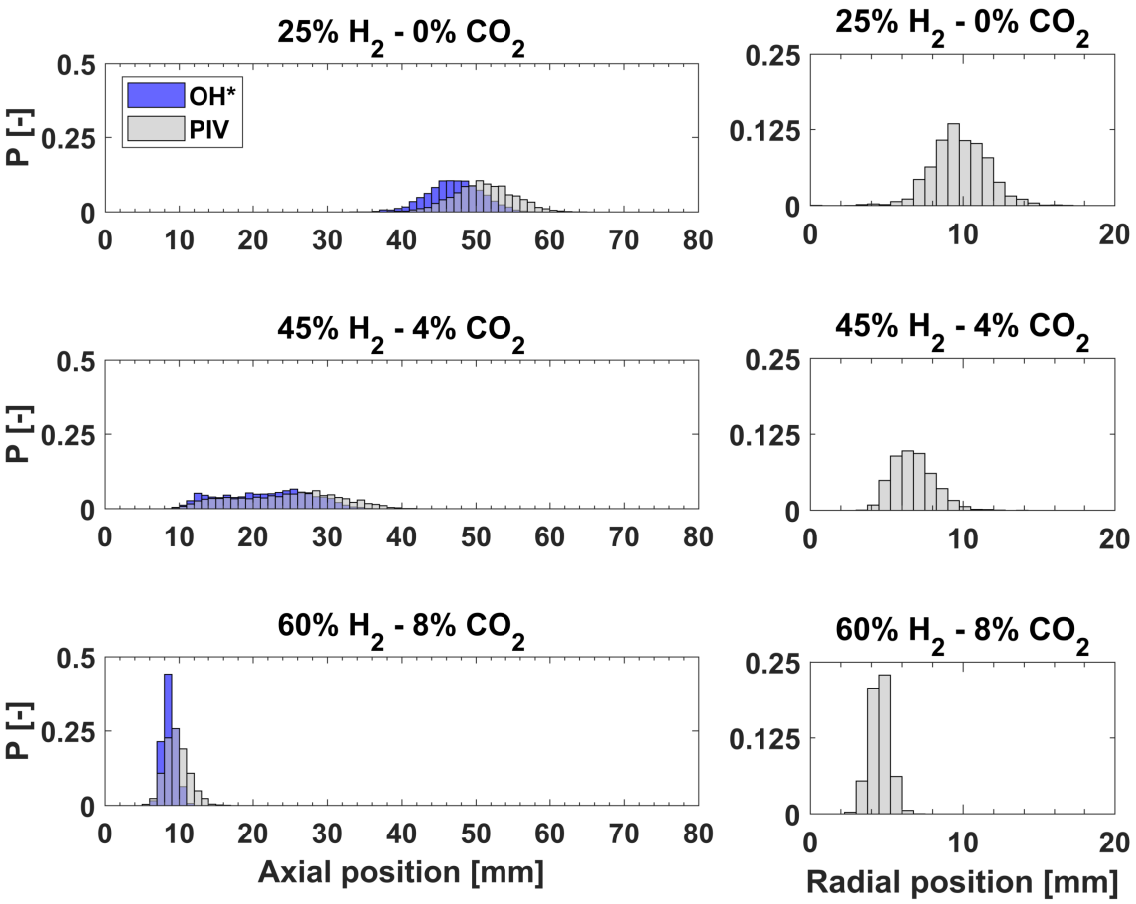

Figure 5.20: Left) PDFs of the lift-off height (blue) and the axial stabilization point location (grey) of the 25% hydrogen flame without CO_2 dilution and the high-hydrogen flame cases. Right) PDFs of radial stabilization point location of the 25% hydrogen flame without CO_2 dilution and the two high-hydrogen flame cases.

Flame case		OH* Axial		PIV Axial		PIV Radial	
		μ [mm]	σ [mm]	μ [mm]	σ [mm]	μ [mm]	σ [mm]
25% H_2	0% CO_2	47.1	3.7	60	4.1	9.8	1.8
45% H_2	4% CO_2	21.6	6.0	24.2	7.0	6.7	1.3
60% H_2	8% CO_2	8.6	0.9	9.6	1.6	4.6	0.6

Table 5.8: Mean and standard deviation of the lift-off height (from OH*) and the axial and radial stabilization point location (from PIV) of the 25% hydrogen flame without CO_2 dilution and the two high-hydrogen flame cases.

5.6. Relative Impact of Hydrogen, CO_2 and Aerodynamics

Figures 5.19 and 5.20 show that the 25% hydrogen flame without CO_2 dilution stabilizes at a more downstream position than the 45% hydrogen - 4% CO_2 flame, which in turn stabilizes at a more downstream position than the 60% hydrogen - 8% CO_2 flame. It appears that the flame stabilizing effects are dominant.

Min and Baillot [27] observe differences in the relative effect of different coflow-diluents including CO_2. They observe more or less equal lift-off heights for flames with identical laminar flame speeds, fuel-jet bulk velocity and coflow bulk velocity. They indicate that the flame stability reduces with increasing fuel-jet bulk velocity. Table 5.5 indicates a steep increase of the bulk velocity of the fuel-jet over the 25% hydrogen flame without CO_2 dilution, the 45% hydrogen - 4% CO_2 flame and

the 60% hydrogen - 8% CO_2 flame. Hence, the stability of the investigated flames is affected by hydrogen fuel-addition, CO_2 coflow-dilution and altered aerodynamics of the fuel-jet and the coflow. In current investigation it seems that the stabilizing effect of hydrogen fuel-addition is significantly larger than the destabilizing effect of the increasing fuel-jet bulk velocity combined with the destabilizing effect of CO_2 coflow-dilution.

6

Conclusions

OH* chemiluminescence and PIV measurements were performed to study the effect of hydrogen fuel-addition and CO_2 coflow-dilution on the stability of a turbulent lifted DNG jet diffusion flame in cold co-flowing air. Both measurement techniques were applied simultaneously at a low sampling frequency of 50 Hz to determine time-averaged statistics of the lift-off height and stabilization point position of the flame. PIV measurements at a high sampling frequency of 2.5 kHz were performed to determine the transient behaviour of the stabilization point, the flow conditions at the stabilization point and the burning velocity.

6.1. Effects of Hydrogen Addition to the Fuel

Hydrogen addition to DNG of a turbulent lifted jet diffusion flame leads to increased flame stability as evidenced from a reduction of the lift-off height and an upstream and radially inward shift of the mean stabilization point location. With increasing hydrogen fuel-addition, the fluctuation of the stabilization point location decreases whilst the frequency of this fluctuation increases.

A model of the stabilization point motion is observed for lifted jet diffusion flames with hydrogen fuel-addition. The stabilization point displacement follows a trajectory in downstream and radially outward direction. This is followed by a sudden jump towards the beginning of a new trajectory at an upstream and radially inward location. The trajectory tends to align with the jet spreading line from the high to low velocity region of the flow. This alignment becomes better with more hydrogen in the fuel. The sudden jumps in stabilization point position are a result of upstream flame islands that merge with the flame edge. The appearance of the flame islands are caused by out-of-plane motion of the flame. The occurrence of sudden jumps hence appearance of flame islands reduces with increasing hydrogen content in the fuel.

Results of the high-speed PIV measurements showed that the burning velocity at the stabilization point increases with increasing hydrogen in the fuel. The burning velocity in terms of S_L is near constant regardless of the hydrogen-fuel content with values between 1.3 S_L and 1.5 S_L. The burning velocity at the stabilization point depends on the direction of the stabilization point motion. For upstream stabilization point motion the burning velocity is $2.7 \leq S_L \leq 3.0$, whereas for downstream stabilization point motion the burning velocity is $0.6 \leq S_L \leq 0.7$. Hydrogen enables the flame to stabilize in flow regions characterized by high axial gas velocity and significant higher levels of vorticity. This effect of hydrogen fuel-addtion becomes stronger with increasing hydrogen in the fuel. The stabilization point is located in the shear layer of the flow, where the transition of high to low gas velocity and vorticity takes place. Very small divergence values are observed upstream of the stabilization point location, indicating incompressible flow.

6.2. Effects of CO_2 Dilution of the Coflow

CO_2 dilution of the coflow of a turbulent lifted jet diffusion flame (with 25% H_2 leads to decreased flame stability. Increasing the amount of CO_2 in the coflow leads to higher lift-off height of the flame and a more downstream and radially outwards stabilization point location. The fluctuation of the stabilization point location increases with more CO_2 in the coflow. The burning velocity at the stabilization point reduces with increasing CO_2 coflow dilution. Significant is the reduction of vorticity at the stabilization point region with CO_2 coflow dilution. Flames with various amounts of hydrogen fuel-addition and CO_2 coflow-dilution but having an identical laminar flame speed do not have similar lift-off heights or stabilization point locations.

6.3. Limitations and Recommendations

The experimental setup used in this study enables the determination of the flame stabilization position, the flow conditions at the stabilization point and the burning velocity. The results of these measurements are proven to be reproducible and of sufficient spatial resolution.

Nonetheless, the setup is unable to determine the actual stabilization point of the flame in the three-dimensional domain, as the OH* and PIV measurements probe the flame along a line-of-sight and in a planar cross-section, respectively. This results in discrepancies between the lift-off height and the axial stabilization point location and a continuous error in the captured transient flame behaviour of the stabilization point. The observed negative burning velocities are an artifact of the latter, next to the appearance of flame island and jumps. The impact of the out-of-plane motion can be reduced by decreasing the time difference Δt between the laser pulses and/or a thicker laser sheet. Applying a stereo-PIV setup can give insight in the out-of-plane flame motion.

The velocity fields extracted from the PIV measurements are inaccurate in the fuel-jet region. The differences in gas velocity of the fuel-jet and the coflow are too large to correctly capture the velocity field in both regions. To increase the accuracy, the PIV measurement should capture solely the stabilization point region.

The setup is unable to investigate flames that stabilize farther downstream of the burner tip than the in this study investigated flames. From this position the seeding particles are unable to visualize the flame base as they are increasingly subjected to draught and dispersion. Improvements can be made in directing the seeding particles towards the flame base by introducing a weak downstream directed airflow and/or a flame enclosure.

Bibliography

[1] M. R. Raupach, G. Marland, P. Ciais, C. Le Quéré, J. G. Canadell, G. Klepper, and C. B. Field, *Global and regional drivers of accelerating CO2 emissions,* Proceedings of the National Academy of Sciences **104**, 10288 LP (2007).

[2] BP, *BP Energy Outlook 2018 edition*, Tech. Rep. (2018).

[3] S. Shafiee and E. Topal, *When will fossil fuel reserves be diminished?* Energy Policy **37**, 181 (2009).

[4] P. M. Cox, R. A. Betts, C. D. Jones, S. A. Spall, and I. J. Totterdell, *Acceleration of global warming due to carbon-cycle feedbacks in a coupled climate model,* Nature **408**, 184 (2000).

[5] J. Warnatz, U. Maas, and R. W. Dibble, *Combustion: Physical and Chemical Fundamentals, Modeling and Simulation, Experiments, Pollutant Formation* (Springer-Verlag Berlin Heidelberg, 2006).

[6] M. Conte, A. Iacobazzi, M. Ronchetti, and R. Vellone, *Hydrogen economy for a sustainable development: state-of-the-art and technological perspectives,* Journal of Power Sources **100**, 171 (2001).

[7] W. McDowall and M. Eames, *Forecasts, scenarios, visions, backcasts and roadmaps to the hydrogen economy: A review of the hydrogen futures literature,* Energy Policy **34**, 1236 (2006).

[8] C. Lawn, *Lifted flames on fuel jets in co-flowing air,* Progress in Energy and Combustion Science **35**, 1 (2009).

[9] K. M. Lyons, *Toward an understanding of the stabilization mechanisms of lifted turbulent jet flames: Experiments,* (2007).

[10] N. Peters and F. Williams, *Liftoff characteristics of turbulent jet diffusion flames,* AIAA Journal **21**, 423 (1983).

[11] L. Vanquickenborne and A. van Tiggelen, *The stabilization mechanism of lifted diffusion flames,* Combustion and Flame **10**, 59 (1966).

[12] J. Buckmaster, *Edge-flames,* Progress in Energy and Combustion Science **28**, 435 (2002).

[13] H. Phillips, *Flame in a buoyant methane layer,* in *Symposium (International) on Combustion*, Vol. 10 (Elsevier, 1965) pp. 1277–1283.

[14] S. Chung, *Stabilization, propagation and instability of tribrachial triple flames,* Proceedings of the Combustion Institute **31**, 877 (2007).

[15] N. J. Moore, J. L. McCraw, and K. M. Lyons, *Observations on Jet-Flame Blowout,* International Journal of Reacting Systems **2008**, 1 (2008).

[16] W. J. Dahm and R. W. Dibble, *Coflowing turbulent jet diffusion flame blowout,* Symposium (International) on Combustion **22**, 801 (1989).

[17] M. Karbasi, *The effects of hydrogen addition on the stability limits of methane jet diffusion flames,* International Journal of Hydrogen Energy **23**, 123 (1998).

[18] Y. Wu, Y. Lu, I. S. Al-Rahbi, and G. T. Kalghatgi, *Prediction of the liftoff, blowout and blowoff stability limits of pure hydrogen and hydrogen/hydrocarbon mixture jet flames,* International Journal of Hydrogen Energy **34**, 5940 (2009).

[19] T. Leung and I. Wierzba, *The effect of hydrogen addition on biogas non-premixed jet flame stability in a co-flowing air stream,* International Journal of Hydrogen Energy **33**, 3856 (2008).

[20] Z. Huang, Y. Zhang, K. Zeng, B. Liu, Q. Wang, and D. Jiang, *Measurements of laminar burning velocities for natural gas-hydrogen-air mixtures,* Combustion and Flame **146**, 302 (2006).

[21] M. Ilbas, A. P. Crayford, I. Yilmaz, P. J. Bowen, and N. Syred, *Laminar-burning velocities of hydrogen-air and hydrogen-methane-air mixtures: An experimental study,* International Journal of Hydrogen Energy **31**, 1768 (2006).

[22] A. Lock, A. M. Briones, S. K. Aggarwal, I. K. Puri, and U. Hegde, *Liftoff and extinction characteristics of fuel- and air-stream-diluted methane-air flames,* Combustion and Flame **149**, 340 (2007).

[23] J. Min, F. Baillot, A. Wyzgolik, E. Domingues, M. Talbaut, B. Patte-Rouland, and C. Galizzi, *Impact of CO2/N2/Ar Addition on the Internal Structure and Stability of Nonpremixed CH4/Air Flames at Lifting,* Combustion Science and Technology **182**, 1782 (2010).

[24] H. Guo, J. Min, C. Galizzi, D. Escudié, and F. Baillot, *A Numerical Study on the Effects of CO2/N2/Ar Addition to Air on Liftoff of a Laminar CH4/Air Diffusion Flame,* Combustion Science and Technology **182**, 1549 (2010).

[25] L. Qiao, Y. Gu, W. J. Dahm, E. S. Oran, and G. M. Faeth, *A study of the effects of diluents on near-limit H2-air flames in microgravity at normal and reduced pressures,* Combustion and Flame **151**, 196 (2007).

[26] L. Qiao, Y. Gan, T. Nishiie, W. J. Dahm, and E. S. Oran, *Extinction of premixed methane/air flames in microgravity by diluents: Effects of radiation and Lewis number,* Combustion and Flame **157**, 1446 (2010).

[27] J. Min and F. Baillot, *Experimental investigation of the flame extinction processes of non-premixed methane flames inside an air coflow diluted with CO 2, N 2, or Ar,* Combustion and Flame **159**, 3502 (2012).

[28] M. Marin and F. Baillot, *Experimental study of the lifting characteristics of the leading-edge of an attached non-premixed jet-flame: Air-side or fuel-side dilution,* Combustion and Flame **171**, 264 (2016).

[29] L. Muñiz and M. G. Mungal, *Instantaneous flame-stabilization velocities in lifted-jet diffusion flames,* Combustion and Flame **111**, 16 (1997).

[30] A. Upatnieks, J. F. Driscoll, C. C. Rasmussen, and S. L. Ceccio, *Liftoff of turbulent jet flames - Assessment of edge flame and other concepts using cinema-PIV,* Combustion and Flame **138**, 259 (2004).

[31] R. L. Gordon, I. Boxx, C. Carter, A. Dreizler, and W. Meier, *Lifted Diffusion Flame Stabilisation: Conditional Analysis of Multi-Parameter High-Repetition Rate Diagnostics at the Flame Base,* Flow, Turbulence and Combustion **88**, 503 (2012).

[32] K. A. Watson, K. M. Lyons, C. D. Carter, and J. M. Donbar, *Simultaneous two-shot CH planar laser-induced fluorescence and particle image velocimetry measurements in lifted CH4/AIR diffusion flames,* Proceedings of the Combustion Institute **29**, 1905 (2002).

[33] A. Joedicke, N. Peters, and M. Mansour, *The stabilization mechanism and structure of turbulent hydrocarbon lifted flames,* Proceedings of the Combustion Institute **30**, 901 (2005).

[34] M. Tacke, D. Geyer, E. Hassel, and J. Janicka, *A detailed investigation of the stabilization point of lifted turbulent diffusion flames,* Symposium (International) on Combustion **27**, 1157 (1998).

[35] J. Oh and Y. Yoon, *Flame stabilization in a lifted non-premixed turbulent hydrogen jet with coaxial air,* International Journal of Hydrogen Energy **35**, 10569 (2010).

[36] L. K. Su, O. S. Sun, and M. G. Mungal, *Experimental investigation of stabilization mechanisms in turbulent, lifted jet diffusion flames,* Combustion and Flame **144**, 494 (2006).

[37] P. R. Medwell, P. A. M. Kalt, and B. B. Dally, *Simultaneous imaging of OH, formaldehyde, and temperature of turbulent nonpremixed jet flames in a heated and diluted coflow,* Combustion and Flame **148**, 48 (2007).

[38] L. D. Arteaga Mendez, M. J. Tummers, E. H. Van Veen, and D. J. Roekaerts, *Effect of hydrogen addition on the structure of natural-gas jet-in-hot-coflow flames,* Proceedings of the Combustion Institute **35**, 3557 (2015).

[39] E. Oldenhof, M. J. Tummers, E. H. van Veen, and D. J. Roekaerts, *Ignition kernel formation and lift-off behaviour of jet-in-hot-coflow flames,* Combustion and Flame **157**, 1167 (2010).

[40] E. W. Lemmon, M. L. Huber, and M. O. McLinden, *NIST Standard ReferenceDatabase 23: Reference Fluid Thermodynamic and Transport Properties - REFPROP. 9.0.* (2010).

[41] Eindhoven University of Technology, *CHEM1D: A one-dimensional laminar flame code,* (2014).

[42] F. T. Nieuwstadt, J. Westerweel, and B. J. Boersma, *Turbulence* (Springer International Publishing, Cham, 2016).